INJECTABLE ALGINATE / DICALCIUM PHOSPHATE CEMENT COMPOSITES FOR BONE TISSUE ENGINEERING

Saliha BİLGİN

T.C
Karabuk University
Institute of Graduate Programs
Department of Biomedical Engineering
Prepared as
Master Thesis

Assist.Prof.Dr. Ammar Zeidan Ghailan ALSHEMARY

KARABUK
June 2020

I certify that in my opinion the thesis submitted by Saliha BİLGİN titled "INJECTABLE ALGINATE / DICALCIUM PHOSPHATE CEMENT COMPOSITES FOR BONE TISSUE ENGINEERING" is fully adequate in scope and in quality as a thesis for the degree of Master of Science.

Assist. Prof. Dr. Ammar Zeidan Ghailan ALSHEMARY .....
Thesis Advisor, Department of Biomedical Engineering

Prof. Dr. Zafer EVİS .....
Thesis Co-Advisor, Department of Engineering Sciences, METU

This thesis is accepted by the examining committee with a unanimous vote in the Department of Biomedical Engineering as a Master of Science thesis. June 25, 2020

Examining Committee Members (Institutions) Signature

Chairman : Prof. Dr. İdris KABALCI (KBU) .....

Member : Assist.Prof.Dr. Ammar Zeidan Ghailan ALSHEMARY (KBU)……...

Member : Prof. Dr. Zafer EVİS (METU) ……..

Member : Prof. Dr. Fatma KANDEMİRLİ (KASU) .....

Member : Assist. Prof. Dr. Hacı Mehmet KAYILI (KBU) ……

The degree of Master of Science by the thesis submitted is approved by the Administrative Board of the Institute of Graduate Programs, Karabuk University.

Prof. Dr. Hasan SOLMAZ .....
Director of the Institute of Graduate Programs

I hereby declare that all information in this document has been obtained and presented in accordance with academic rules and ethical conduct. I also declare that, as required by these rules and conduct, I have fully cited and referenced all material and results that are not original to this document.

Saliha BİLGİN

ABSTRACT

M. Sc. Thesis

INJECTABLE ALGINATE / DICALCIUM PHOSPHATE CEMENT COMPOSITES FOR BONE TISSUE ENGINEERING

Saliha BİLGİN

Karabük University
Institute of Graduate Programs
The Department of Biomedical Engineering

Thesis Advisor:
Assist. Prof. Dr. Ammar Zeidan Ghailan ALSHEMARY

Co-Advisor:
Prof. Dr. Zafer EVİS
June 2020, 60 pages

Biocompatible dicalcium phosphate (DCP) cement have been widely used for fixing orthopaedic implants. In this thesis, it was aimed to investigate the impact of sodium alginate (SA) addition of different amounts on microstructural, mechanical, and biological properties of DCP cement. β-Tricalcium phosphate (β-TCP) was prepared using a microwave-assisted wet precipitation method. The lattice parameters of the obtained particles determined from X-ray diffraction (XRD) patterns, were in good match with a standard phase of β-TCP. Field emission scanning electron microscopy (FESEM) examination revealed that the particles were in globular shape. Furthermore, all functional groups of β-TCP were also detected in Fourier-transform infrared spectroscopy (FTIR) spectra. A pure phase of DCP cement was prepared

using monocalcium phosphate monohydrate (MCPM) / β-TCP powder mixture mixed with a calculated amount of water. SA/DCP cement composites were prepared by dissolving different amounts of SA into the liquid phase (water) to obtain different final concentrations (0.5%, 1.0%, 2.0% and 3.0%). The prepared cements were characterized with XRD, SEM, FTIR and Thermogravimetric analysis (TGA) techniques. XRD results showed that pure DCP and SA/DCP cements were in good match with Monetite phase. SEM results confirmed that addition of SA inhibited growth of DCP particles. Setting time and injectability behaviour were increased significantly upon increasing SA amount into DCP cements. *In vitro* biodegradation analysis was evaluated using Simulated body fluid (SBF) over 21 days at 37 ºC. The highest cumulative weight loss (%) in SBF was observed for 2.0% SA/DCP (about 26.52%) after 21 days of incubation. Amount of Ca^{2+} ions released in SBF increased with the addition of SA. DCP and SA/DCP cements showed the highest mechanical strength after 3 days of incubation in SBF and declined with prolonged immersion periods. *In vitro* cell culture studies were conducted using Dental pulp stem cells (DPSCs). Viability and morphology of cells incubated in extracts media of DCP and SA/DCP discs after 24 h incubation was studied with MTT assay and fluorescence microscopy imaging, respectively. All prepared cements were cytocompatible and viability of cells incubated in extracts of cements was higher than observed in the control group. Based on the outcomes, SA/DCP bone cements have a promising future to be used as a bone filler.

Key Words: Biomedical biomaterials; Dicalcium phosphate cement; Sodium alginate; Setting time; Mechanical properties; *In vitro* cell culture analysis.

Science Code: 92503

ÖZET

Yüksek Lisans Tezi

KEMİK DOKU MÜHENDİSLİĞİ İÇİN ENJEKTE EDİLEBİLİR ALJİNAT / DİKALSİYUM FOSFAT ÇİMENTO KOMPOZİTLERİ

Saliha BİLGİN

Karabük Üniversitesi
Lisansüstü Eğitim Enstitüsü
Biyomedikal Mühendisliği Anabilim Dalı

Tez Danışmanı:
Dr.Öğr.Üyesi Ammar Zeidan Ghailan ALSHEMARY

İkinci Danışmanı:
Prof. Dr. Zafer EVİS
Haziran 2020, 60 sayfa

Biyouyumlu dikalsiyum fosfat (DCP) çimentolar ortopedik implantları sabitlemek için yaygın olarak kullanılmaktadır. Bu tezde farklı miktarlarda sodyum aljinat (SA) ilavesinin DCP çimentolarının mikroyapısal, mekanik ve biyolojik özellikleri üzerindeki etkisini araştırma amaçlanmıştır. Beta-trikalsiyum fosfat (β-TCP) mikrodalga destekli ıslak çökeltme yöntemi kullanılarak hazırlanmıştır. Elde edilen parçacıkların X-ışını kırınımından (XRD) belirlenen latis parametreleri, standart bir β-TCP fazı ile iyi eşleşmiştir. Alan emisyonlu taramalı elektron mikroskobu (FESEM) incelemesi, parçacıkların küresel şeklinde olduğunu ortaya koymuştur. Ayrıca, Fourier-dönüşümlü kızılötesi spektroskopisi (FTIR) spektrumlarında β-TCP'nin tüm fonksiyonel grupları da tespit edilmiştir. DCP çimentosunun saf bir

fazı, hesaplanan miktarda su ile karıştırılmış monokalsiyum fosfat monohidrat (MCPM) / β-TCP toz karışımı kullanılarak hazırlanmıştır. Sodyum aljinat (SA) / DCP çimento kompozitleri, farklı nihai konsantrasyonları (%0.5, %1.0, %2.0 ve %3.0) elde etmek için farklı miktarlarda SA'yı sıvı fazda (su) eriterek hazırlanmıştır. Hazırlanan çimentolar XRD, SEM, FTIR ve Termogravimetrik analiz (TGA) ile karakterize edilmiştir. XRD sonuçları saf DCP ve SA/DCP çimentolarının Monetit fazı ile iyi eşleştiğini göstermiştir. SEM sonuçları, SA ilavesinin DCP partiküllerinin büyümesini inhibe ettiğini doğrulamıştır. Priz süresi ve enjekte edilebilirlik davranışı, DCP çimentolarına SA miktarının arttırılmasıyla önemli ölçüde artmıştır. *In vitro* biyodegradasyon, 37 °C'de 21 gün boyunca Simüle edilmiş vücut sıvısı (SBF) kullanılarak değerlendirilmiştir. SBF'de en yüksek kümülatif ağırlık kaybı (%), 21 günlük inkübasyondan sonra %2.0 SA/DCP (yaklaşık %26.52) için gözlenmiştir. SBF'de salınan Ca^{2+} iyonlarının miktarı, SA ilavesiyle artmıştır. DCP ve SA/DCP çimentoları SBF'de 3 günlük inkübasyondan sonra en yüksek mekanik dayanıklılığı göstermiştir ve uzun süreli daldırma periyotlarıyla azalmıştır. *In vitro* hücre kültürü çalışmaları dental pulpa kök hücreleri (DPSC) kullanılarak gerçekleştirilmiştir. DCP ve SA/DCP disklerinin özlerinde 24 saatlik inkübasyondan sonra hücrelerin canlılığı ve morfolojisi sırasıyla MTT analizi ve floresans mikroskopi görüntüleme ile incelenmiştir. Tüm çimentolar hücre uyumluydu ve çimento özlerinde inkübe edilen hücrelerin yaşayabilirliği kontrol grubunda gözlemlenenden daha yüksekti. Sonuçlara dayanarak, SA/DCP kemik çimentolarının kemik dolgu maddesi olarak kullanılması umut verici bir geleceğe sahiptir.

Anahtar Kelimeler: Biyomedikal biyomalzemeler; Dikalsiyum fosfat çimento; Sodyum aljinat; Priz süresi; Mekanik özellikler; *In vitro* hücre kültürü analizleri.

Bilim Kodu **:** 92503

ACKNOWLEDGEMENT

I would like to express my sincere gratitude and appreciation to my research supervisors Assist. Prof. Dr. Ammar Zeidan Ghailan ALSHEMARY for his guidance, support, and patience towards the completion of this work. He provided me with very valuable ideas, advices, and suggestions to complete this research work. I am extremely grateful to my co-supervisor, Prof. Dr. Zafer EVİS. He has been a tremendous mentor and guides for me. I would like to thank him for encouraging my research. I would also like to my sincere thanks to Prof. Dr. Ayşen TEZCANER for her help during this work and for allowing me to use tissue culture facilities.

I am also greatly obliged to Karabük University for providing financial support via Project no. KBÜBAP-18-YL-178. I am very much thankful to Biomaterials Laboratory, Department of Engineering Sciences at Middle East Technical University for providing facilities to complete this thesis. I am deeply appreciative to my research fellows: Gülhan IŞIK and Ali MOTAMENI for their continuous help and support during this research work.

Special thanks to my husband, my mother and my father for supporting me every time.

CONTENTS

Page

Page

Page

LIST OF FIGURES

Page

Page

LIST OF TABLES

Page

SYMBOLS and ABBREVIATIONS

SYMBOLS

°	: Degree
°C	: The degree Celsius
µL	: Microliter
3D	: Three Dimensional
Å	: Angstrom
a-axis	: lattice parameter
b-axis	: lattice parameter
c-axis	: lattice parameter
C	: Carbon
Ca	: Calcium
Cl	: Chlorine
cm	: Centimeter
D_{th}	: Theoretical density
g	: Gram
h	: Hour
H	: Hydrogen
*I*a	: Monoclinic space group
K	: Potassium
kg	: Kilogram
kN	: Kilonewton
L	: Liter
Mg	: Magnesium
Min	: Minute
mL	: milliliter
MPa	: Megapascal
N	: Nitrogen

Na : Sodium

nm : Nanometer

O : Oxygen

P : Phosphorus

*P*1 : Triclinic space group

P_{21}/a : Monoclinic space group

$P6_3/mmc$: Hexagonal space group

ppm : Parts per million

R3c : Rhombohedral space group

rpm : Revolutions per minute

S : Sulfur

sec : Second

V : Cell volume

V_0 : Volume per formula unit

v/v : Volume/volume

W : Watt

w/v : Weight/volume

Z : Number of formula units per cell

α : Alpha, cell angle

β : Beta, cell angle

γ : Gamma, cell angle

2θ : The diffraction angle

ρ : Density

Φ : Porosity

ABBREVIATIONS

ASTM	: American Society for Testing and Materials
BSA	: Bovine Serum Albumin
CPs	: Calcium Phosphates
DAPI	: 4′,6-diamidino-2-phenylindole
DCP	: Dicalcium Phosphate
DCPA	: Dicalcium Phosphate Anhydrous
DCPD	: Dicalcium Phosphate Dihydrate
DMEM	: Dulbecco's Modified Eagle's Medium
DPSCs	: Dental Pulp Stem Cells
FBS	: Fetal Bovine Serum
FDA	: American Food and Drug Administration
FESEM	: Field Emission Scanning Electron Microscopy
FT	: Final Time
FTIR	: Fourier Transform Infrared Spectroscopy
HA	: Hydroxyapatite
ICP-OES	: Inductively Coupled Plasma-Optical Emission Spectrometry
IT	: Initial Time
JCPDS	: Joint Committee on Powder Diffraction and Standards
MCPA	: Mono Calcium Phosphate Anhydrous
MCPM	: Mono Calcium Phosphate Monohydrate
MMA	: Methyl Methacrylate
MTT	: 3-(4,5-dimethylthiazole-2-yl)-2,5-diphenyltetrazolium bromide
PBS	: Phosphate Buffered Saline
PMMA	: Poly (Methyl Methacrylate)
SA	: Sodium Alginate
SBF	: Simulated Body Fluid
SEM	: Scanning Electron Microscopy
TCP	: Tricalcium Phosphate

TGA	: Thermo Gravimetric Analysis
XRD	: X-Ray Diffraction
α-TCP	: α - Tricalcium Phosphate
α′-TCP	: α′ - Tricalcium Phosphate
β-TCP	: β - Tricalcium Phosphate

CHAPTER 1

INTRODUCTION

1.1. BONE STRUCTURE

Bone is a mineralized connective tissue and protects numerous vital organs and soft tissues. Bone is classified based on its structure for two types (i) cortical (compact) bone and (ii) trabecular (cancellous) bone. Compact bone makes the outer surfaces of the bones, and it is denser than trabecular bone with 5 to 10% porosity (Zhang et al., 2007). Trabecular bone with a 50 to 90% porosity is very porous and softer than compact bone (Zhang et al., 2007). Bone is mainly composed of a collagen and calcium phosphates (CPs) composites that gives shape to the skeleton of the body. Bone has a honeycomb-like matrix inside that helps to supply the bone rigidity. Bone possess three types of cells: (i) **Osteoblasts:** These are derived from mesenchymal stem cells, making new bone matrix known as osteoid via osteogenesis process (Martin, 2003). (ii) **Osteocytes:** They are inactive osteoblasts, establishing connections between osteocytes and osteoblasts. (iii) **Osteoclasts:** They are derived from the hematopoietic lineage and responsible for osteolysis process (Hattersley et al., 1991). These cells dissolve the mineral of bone and destroy the organic matrix (Martin, 2003). Hierarchical organization of bone from the macro to the sub-nanoscale was illustrated in Figure 1.1.

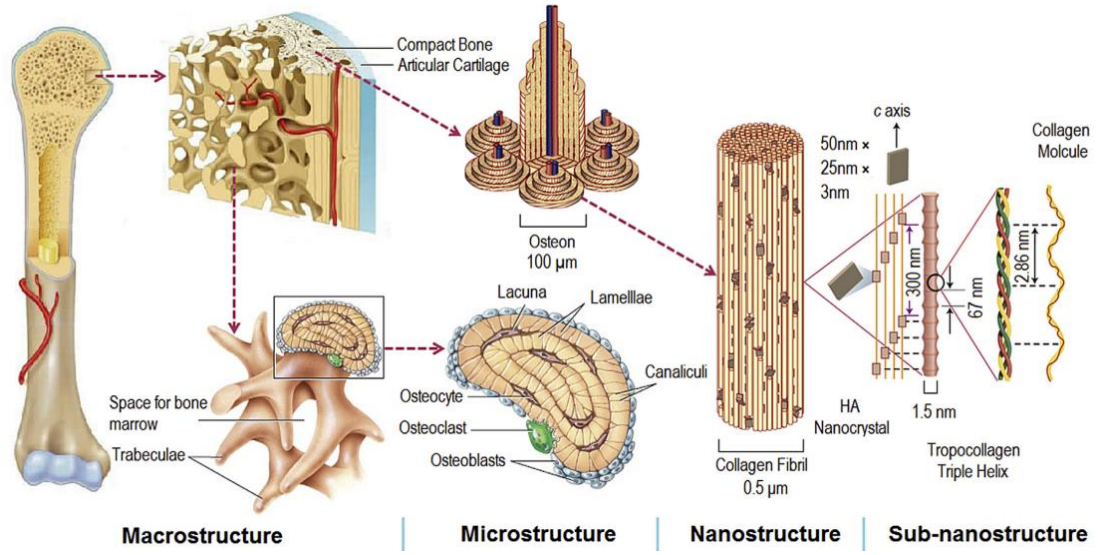

Figure 1.1. Hierarchical organization of bone from the macro to the sub-nanoscale (Wang et al., 2016b).

1.2. CEMENTS AS BONE REPAIR MATERIALS

Bone cements are widely used for implant fixation in several trauma orthopedic surgeries (Vaishya et al., 2013). Their preparation is based on chemical reaction that takes place between the powder phase and the liquid phase, which results in paste formation as an intermediate stage. After this stage, it self-sets once implanted in the body. This implies that the material is flexible, which guarantees ideal fit on the implanted site providing high bone–material contact, even in strong geometric deformities. However, the way that the bone cements experience a setting response once embedded and framing a hard structure ensure a specific degree of mechanical support. This mechanical support could change based on cement type used. Latest developments in orthopedic surgery focus on use of minimally invasive surgical techniques (Ginebra & Montufar, 2019). However, there is no ideal cement in the medical market; nowadays all bone cements have some limitations. Bone cements divided into two main classes, acrylic bone cements and dicalcium phosphate (DCP) cements.

1.2.1. Acrylic Bone Cements

Poly (methyl methacrylate) (PMMA) used as acrylic bone cement, is one of the most common bone cement material used in orthopedic surgeries, dental applications, vertebroplasty and kyphoplasty. However, it has some limitations. PMMA polymerization is an exothermic reaction. The temperature rises about to 60-120 °C causing serious thermal damage surrounding the bone tissue (McMahon et al., 2012). Additionally, there is also concern about severe toxicity because of methyl acrylate monomer (MMA) (Pikis et al., 2015). The liquid monomer (MMA) can cause asthmatic reactions or lacrimation (Lewis, 1997). Furthermore, it was shown that monomers left decreased the growth rate of osteoblasts compared to other common materials, such as CPs and hydroxyapatite (HA) (Ricker et al., 2008).

1.2.2. Dicalcium Phosphate Cements

Dicalcium Phosphate (DCP) Cements have been suggested as an alternative option for PMMA. It has several advantages over PMMA like its good biocompatibility, capability of self-hardening at room temperature and causing no exothermic effect during the hardening process. Due to biocompatibility and ability to degrade inside the body that encourages bone growth, it is used in bone replacement in oral surgery and craniofacial applications and osteonecrotic sites in the body (Ambard & Mueninghoff, 2006). However, it has poor mechanical properties along with a low degradation rate (Julien et al., 2007). Some polymers such as alginate, chitin, chitosan, cellulose, collagen, gelatine and synthetic polymers have been used to improve properties like porosity, injectability, degradation rate and mechanical properties (Perez et al., 2012).

1.3. PROBLEM STATEMENT

DCP cements widely used for various applications of bone regeneration such as craniofacial and maxillofacial reconstruction (skull base defect repair, cranioplasty, augmentation genioplasty, cranial recontouring, on-lay grafting, cranial flap augmentation) (Gómez et al., 2005). However, it has poor mechanical properties

along with a low degradation rate (Julien et al., 2007).

1.4. OBJECTIVES OF THE THESIS

Generally, the main objectives of this research project are to investigate and improve the microstructural, mechanical, and biological properties of DCP cements using Sodium alginate (SA) as an additive.

Here the aim of this thesis can be summarized as,

- To synthesize β-Tricalcium phosphate (β-TCP) based biomaterials using microwave-assisted precipitation method and to characterize the above-mentioned β-TCP material utilizing XRD, FTIR, SEM and ICP-OES techniques.
- To synthesize DCP cements from the corresponding β-TCP precursors incorporated with different compositions of alginate and to characterize the obtained cements utilizing XRD, FTIR, FESEM, TGA and ICP-OES techniques.
- To evaluate the impact of alginate substitution up to the setting time, injectability and physicochemical properties of DCP cements.
- To study the effect of alginate substitution on the *in vitro* resorption and degradation of the DCP cements in simulated body fluid (SBF).
- To study the effect of alginate substitution on the mechanical properties of the DCP cements in SBF.
- To study the effect of alginate substitution on the *in vitro* osteoinduction, osteoconduction and osseointegration properties of the DCP and Alginate - DCP cements cultured with Dental pulp stem cells (DPSCs).

1.5. SIGNIFICANCE OF THE THESIS

Physicochemical properties of DCP cements play an important role in predicting *in vivo* performance of these materials. Cements injectability is important for invasive surgical techniques for filling bone defects; however, due to the liquid-solid stage

division, DCP cements without additives usually have the weak infusing ability. Sodium alginate (SA) can be used to improve injectability, physicochemical and mechanical properties of DCP cements. Controlling the resorption parameters of DCP cements, it may be easily feasible to control the flow of bone stimulating ions. In this thesis, it was aimed to investigate the effect of SA addition of different amounts on microstructural, mechanical, and biological properties of DCP cements. The synthesis of materials proposed in this thesis is a modest effort to produce biomedical materials, which will significantly reduce their cost and make them available to ordinary citizens at an affordable rate.

CHAPTER 2

LITERATURE REVIEW

2.1. CALCIUM PHOSPHATES

CPs highly resemble with the mineral part of the bone and tooth. It is classified based on Ca/P ratios (Table 2.1) and frequently used as bone graft material.

Table 2.1. Main CPs forms (Bohner, 2010).

Name	Formula	Ca/P ratio	Mineral	Symbol
Monocalcium phosphate monohydrate	$Ca(H_2PO_4)_2 \cdot H_2O$	0.50	-	MCPM
Dicalcium phosphate	$CaHPO_4$	1.00	Monetite	DCP
Dicalcium phosphate dihydrate	$CaHPO_4 \cdot 2H_2O$	1.00	Brushite	DCPD
Octocalcium phosphate	$Ca_8H_2(PO_4)_6 \cdot 5H_2O$	1.33	-	OCP
Precipitated hydroxyapatite	$Ca_{10-x}(HPO_4)_x(PO_4)_{6-x}(OH)_{2-x}$	1.33-1.67	-	PHA
Precipitated amorphous calcium phosphate	$Ca_3(PO_4)_2 \cdot nH_2O$ where n = 3,4,5; 15-20% H_2O	0.67-1.50	-	ACP
Monocalcium phosphate	$Ca(H_2PO_4)_2$	0.50	-	MCP
α-Tricalcium phosphate	$\alpha\text{-}Ca_3(PO_4)_2$	1.50	-	α-TCP
β-Tricalcium phosphate	$\beta\text{-}Ca_3(PO_4)_2$	1.50	-	β-TCP
Sintered hydroxyapatite	$Ca_{10}(PO_4)_6(OH)_2$	1.67	Hydroxy apatite	SHA
Oxyapatite	$Ca_{10}(PO_4)_6O$	1.67	-	OXA
Tetracalcium phosphate	$Ca_4(PO_4)_2O$	2.00	Hilgen stockite	TTCP

2.1.1. Monocalcium Phosphate Monohydrate

Monocalcium phosphate monohydrate (MCPM, $Ca(H_2PO_4)_2 \cdot H_2O$) is a very good water-soluble material resulted in low pH value. MCPM has a stable phase at a pH below 2.5 (Ginebra, 2008). Due to its high solubility and acidity nature, MCPM is not preferred to be used in biomedical applications. Drying the MCPM at 100 °C leads to evaporation of water molecule forming anhydrous form (MCPA). The density of MCPA is higher than that of MCPM (Farahani et al., 2012). However, MCPM is used as a source of DCP cements and the last used in dental, drug delivery and biomedical applications (Kouassi et al., 2003; Taha et al., 2017; Shu et al., 2019).

2.1.2. Dicalcium Phosphate

DCP materials are a kind of CPs with a Ca/P ratio of 1.0 (Kossler & Fuchs, 2009), commonly used in orthopedic and dental applications. Furthermore, they are used as a food additive and as a polishing agent in toothpaste (Dorozhkin & Epple, 2002; Qadir et al., 2014). Dicalcium phosphate dihydrate (DCPD, $CaHPO_4 \cdot 2H_2O$) cements and dicalcium phosphate anhydrous (DCPA, $CaHPO_4$) are two forms of DCP cements widely used as bone fillers. DCPD transforms into DCPA at temperatures above ~80 °C

2.1.2.1. Dicalcium Phosphate Anhydrous

Dicalcium Phosphate Anhydrous (DCPA) is known as monetite, it is used to enhance skeletal repair (Desai et al., 2007), also used in orthopedic applications (Koju et al., 2018), drug delivery applications (Taha et al., 2017), dental applications (El Briak et al., 2008) and craniofacial bone augmentation (Tamimi et al., 2009a). DCPA cements was synthesized using different methods such as; hydrothermal method (Jinawath et al., 2001), precipitation from microemulsion (Kong et al., 2005), crystallization from solution (Sivakumar et al., 1998), electro and chemical deposition (Rohanizadeh & LeGeros, 2008) and microwave-assisted method (Kohn et al., 2002). DCPA crystallizes with a space group of *P*l which is in triclinic crystal

system and unit-cell parameters of a=6.910 Å, b=6.627 Å, c=6.998 Å , α=96.34º, β=103.82º and γ= 88.33º as seen in Figure 2.1 (Mathew & Takagi, 2001). DCPA is stable at a pH range of 2.5 - 4.2 (Ginebra, 2008). However, DCPA converts to HA when pH is changed to a physiological pH of 7.4. Furthermore, it is more stable than DCPD above 121 °C. Monetite's crystal growth rate is slow, so DCPD forms easier than DCPA. The density of DCPA is 2.93 g/cm^3 (Unosson et al., 2015). As with DCPD, the solubility of DCPA is pH dependent. Moreover, its solubility decreases with increasing the temperature.

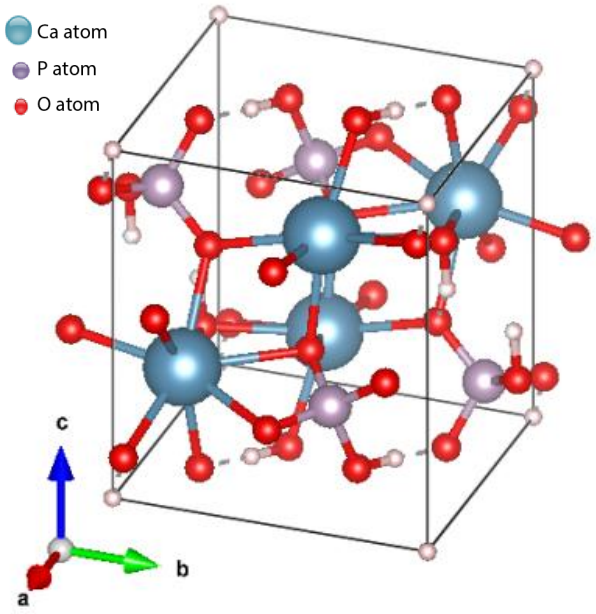

Figure 2.1. The unit cell structure of DCPA.

2.1.2.2. Dicalcium Phosphate Dihydrate

Dicalcium phosphate dihydrate (DCPD) is known as brushite, it is used for maxillofacial bone augmentation (Tamimi et al., 2009b), treatment of periodontal diseases (Tamimi et al., 2008), drug delivery applications (Taha et al., 2017), osteoplastic surgery (Fomin et al., 2017) and cranial defects (Ji & Ahn, 2010). DCPD crystallizes with a space group of *Ia* which is in monoclinic crystal system and unit cell parameters of a=5.812 Å, b=15.180 Å, c=6.239 Å and β=116.42° as seen in Figure 2.2 (Dumitraş et al., 2004). The density of DCPD is 2.33 g/cm^3 (Unosson et al., 2015). Heat-treatment of DCPD leads to loss of water molecule,

forming an anhydrous form of DCPA (Klammert et al., 2009).

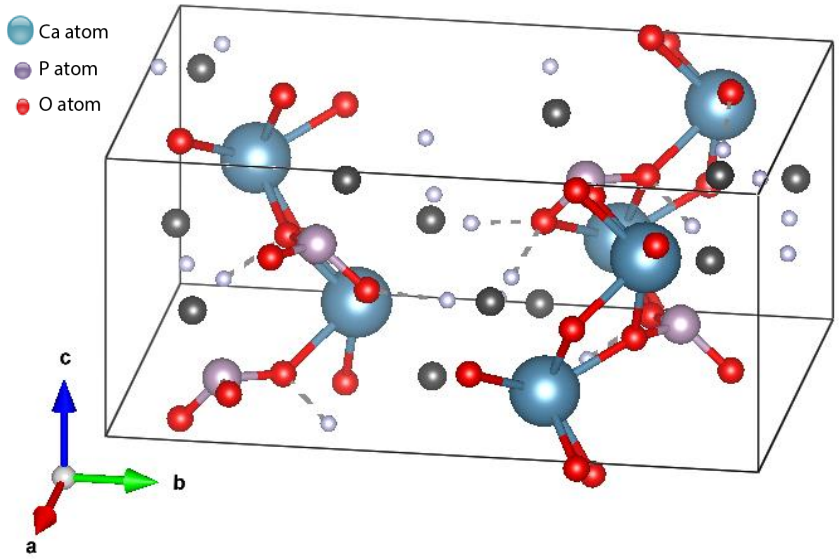

Figure 2.2. The unit cell structure of DCPD.

2.1.3. Tricalcium Phosphate

Tricalcium phosphate (TCP, $Ca_3(PO_4)_2$) is well known biomaterial and commonly used in the biomedical area. It is used in particular to treat bone defects, repairing devices and as coatings on metal alloy prostheses. TCP introduces three polymorphs with stage change temperatures. β-TCP (rhombohedral) transforms to α-TCP (monoclinic) at 1125 °C and α-TCP converts to α′-TCP (hexagonal) at 1430 °C (Moreno et al., 2019) according to Kreidler and Hummel's phase diagram (Kreidler & Hummel, 1967) as shown in Table 2.2.

Table 2.2. Structural data of TCP polymorphs.

Property	TCP Polymorphs		
	β-TCP (Yashima et al., 2003)	**α-TCP** (Yashima & Sakai, 2003)	**α'-TCP** (Yashima & Sakai, 2003)
Symmetry	Rhombohedral	Monoclinic	Hexagonal
Space group	R3c	$P2_1/a$	$P6_3/mmc$
a (Å)	10.4352	12.859	5.3507
b (Å)	10.4352	27.354	5.3507
c (Å)	37.4029	15.222	7.684
α (°)	90	90	90
β (°)	90	126.35	90
γ (°)	120	90	120
Z	21	24	1
V (nm^3)	3.5272	4.31	0.19052
V_0 (nm^3)	0.1680	0.180	0.19052
D_{th} (g/cm^3)	3.066	2.866	2.702

2.1.3.1. β - Tricalcium Phosphate

β - Tricalcium Phosphate (β-TCP, β-Ca_3 $(PO_4)_2$) has seen much broader use as a biodegradable CPs or as a part of biphasic CPs in the form of dense or macroporous granules or scaffolds in clinical applications (Rahaman, 2014). Based on the crystal structure (Figure 2.3), β-TCP has R3c space group which in a rhombohedral structure with unit cell parameters of a=b=10.4352 Å and c=37.4029 Å with α=β=90°, γ=108.65°. It has a density of 3.07 g/cm^3 (Mirhadi et al., 2011). β-TCP has complex structures consisting of tetrahedral phosphate centres connected to calcium ions with oxygen.

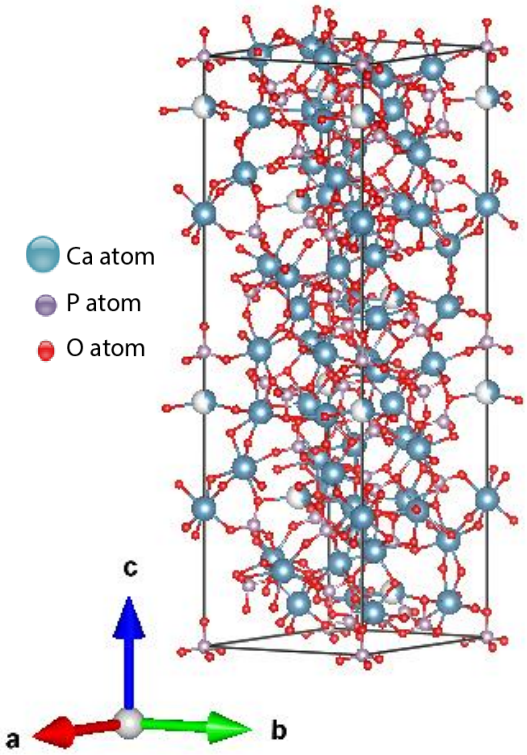

Figure 2.3. The unit cell structure of β-TCP.

Methods to Synthesize β-TCP Particles

Different methods have been used to synthesis pure phase of β-TCP, such as: electrochemical (Djošić et al., 2008), micro-emulsion (Dai et al., 2016), sonochemical (De Campos et al., 2007), hydrothermal (Gan et al., 2019), sol-gel (Sanosh et al., 2010) and microwave-assisted method (Taha et al., 2017). Wet chemical method (Fathi et al., 2015; Chang, 2016) has also been used for the production of HA nanoparticles. A brief detail of these methods is given below.

I. Wet precipitation method

Wet precipitation method is one of the most used techniques to prepare β-TCP powders. This method involves the mixing of Ca^{2+} and PO_4^{3-} based precursors in a basic or neutral solution to prepare poorly crystalline β-TCP. Main advantages of using wet precipitation methods are; easy to process, no need for complex devices, having low reaction time and temperatures, low-cost raw materials, controllable

particle morphology and the mean size, high purity materials, scalability, reproducibility, possible for industrial application and synthesis conditions can be easily controlled (Ramesh et al., 2013; Krauklis et al., 2018; Rodríguez-Lugo et al., 2018).

II. Microwave-assisted wet precipitation method

Some benefits of using microwave are these superheating increases the reaction rate and enables faster synthesis, shape and size control by easily adjusting reaction parameters and because of better controlling of process parameters, greater reproducibility of chemical reactions than in conventional heating (Saleh et al., 2017). On the other hand, some of the limitations of using microwave have been observed such as lack of scalability, limited applicability for materials that absorb microwave and safety and health hazards about using of a microwave oven (Saleh et al., 2017).

III. Sol-gel method

A “Sol” is a scattering of colloidal amorphous or crystalline particles. A “Gel” is a 3D interconnected network shaped by sol particles. Sol-gel term refers to the processes of gels produced from colloidal suspensions. This process includes the production of inorganic matrices by the arrangement of colloidal suspension and shaping a bunch of gels. After drying it converts into xerogel shape (Aurobind et al., 2006). In sol-gel chemistry, hydrolysis and condensation reactions transform to molecular precursors.

The sol-gel method generally consists of the following basic steps: Hydrolysis of precursor, polycondensation, gelation, aging, drying and high-temperature process (Aurobind et al., 2006).

IV. Solid-state reaction method

Several forms of CPs particles can be synthesized using a solid-state method, the solid precursors are mixed and grinded in wet media to make the homogeneous mixture and reduce particle size. For wetting medium distilled water is used. At appropriate temperature solid-state reaction is carried out between the starting materials. This process is known as calcination. Calcination makes the starting precursors interact with them and results in a homogeneous phase. After calcination, the powder is shaped then it is densified with sintering. Sintering is a process of heating the material to increase its grain size and strength by bonding together the particles.

V. Hydrothermal method

In this method, from room temperature to high-temperature nanoparticles can be made. Depending on the vapour pressure of the principal components in the reaction, low pressure or high-pressure conditions are used to monitor the morphology of the materials to be prepared. The advantages of hydrothermal synthesis are at low-temperature materials with good crystallinity and homogeneous size and shape properties (Zhang & Vecchio, 2007).

2.2. ALGINATE AND ITS IMPORTANCE

Alginate is the foremost plenty of marine biopolymer within the world following to cellulose. The main alginate source is found in the cell walls and intercellular regions of marine brown algae such as *Ascophyllum nodosum, Macrocystis pyrifera and Laminaria hyperborea* (Shilpa et al., 2003). The alginate molecules provide flexibility and strength for the plant growth in the sea. Some bacteria synthesize alginate like *Azotobacter* and *Pseudomonas species* (Rani et al., 2019). Alginate exsited in different kinds such as: sodium alginate (SA), alginic acid, potassium, calcium and ammonium salts, an ester of alginic acid and propylene glycol alginate (Venkatesan et al., 2014) and SA consider the main type of alginate (McHugh, 2003).

Alginate is a linear and anionic polysaccharide and formed by the whole family of linear copolymers containing blocks of β-D-mannuronic acid (M) and (1,4) linked α-L-guluronic acid (G) where these blocks are constituted by sequential G residues (GGGG), sequential M residues (MMMM) and also mixed G and M residues (GMGM) (Lee & Mooney, 2012). The structure of alginate blocks is given in Figure 2.4.

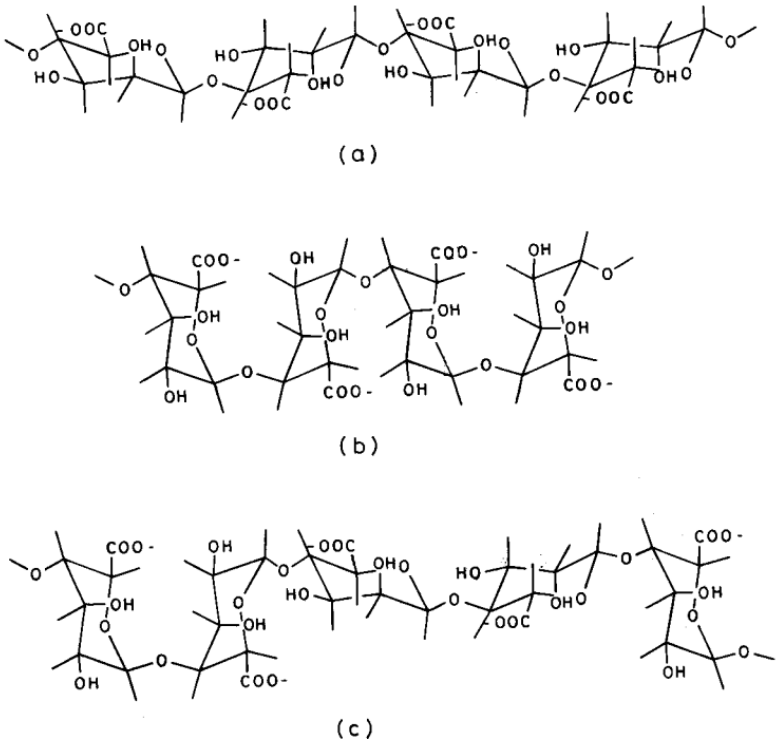

Figure 2.4. The structure of a) β-D-Mannuronic acid (M block), b) α-L-Guluronic acid (G block) and c) mixed block (Shilpa et al., 2003).

Sodium Alginate (SA), a well-known polymer-based biomaterial, has been frequently used in the medical sector due to its biocompatibility and ease of gelation. SA in hydrogel form has been especially appealing in tissue engineering applications. Furthermore, these gels hold basic similarity to the extracellular networks in tissues (Lee & Mooney, 2012). Multivalent cations are regularly utilized to make crosslinks among carboxyl and hydroxyl moieties on neighbouring polysaccharide chains. Previous studies deduced that addition of SA improved mechanical properties of the composites. Zhang et al. (2013) found compressive modulus and the compressive yield strength of the nano-HA/collagen composites

increased as SA content was increased. Yu et al. (2019) revealed that SA can successfully improve compressive resistance and elasticity properties of κ-carrageenan composite gel. Dabiri et al. (2019) demonstrated that addition of 0.5% SA increased the elastic modulus and compressive strength of undoped brushite cement. Furthermore, numerous studies confirmed that adding SA to materials improves adhesion and proliferation of cells (Turco et al., 2009; Dabiri et al., 2019; Ni et al., 2019)

2.3. DENTAL PULP STEM CELLS (DPSCs)

Dental pulp stem cells (DPSCs) are obtained from the teeth recovered during a normal dental procedure. DPSCs can be isolated, cultured, and cryopreserved. DPSCs have an extremely proliferative ability and probability of differentiation into a variety of cells. Additionally, more than 80 passages can be passed with the capacity to protect differentiation (Laino et al., 2006). The osseo-specific markers of DPSCs are alkaline phosphatase (ALP), osteopontin and osteocalcin. In this thesis, DPSCs were used for cell culture tests.

CHAPTER 3

METHODOLOGIES

3.1. MATERIALS AND CHEMICALS

Calcium nitrate tetrahydrate ($Ca(NO_3)_2 \cdot 4H_2O$, Merck-Germany), di-Ammonium hydrogen phosphate ($(NH_4)_2HPO_4$, Merck-Germany), Sodium chloride (NaCl, Merck-Germany), Sodium hydrogen carbonate ($NaHCO_3$, Merck-Germany), Potassium chloride (KCl, Merck-Germany), Potassium Hydrogen Phosphate Trihydrate (K_2HPO_4. $3H_2O$, Merck-Germany), Magnesium Chloride Hexahydrate ($MgCl_2$. $6H_2O$, Merck-Germany), Hydrogen chloride (1.0M–HCl, Merck-Germany), Calcium chloride ($CaCl_2$, Merck-Germany), Sodium sulfate (Na_2SO_4), Tris (hydroxymethyl) aminomethane and Dimethyl sulfoxide (Merck-Germany) Monocalcium phosphate monohydrate (MCPM, Merck-Germany). Sodium Alginate (SA), o-cresolphthalein complex one, 8-hydroxyquinaline-5-sulfonic acid, 2-amino-2-methyl-1-propanol and Thiazolyl Blue tetrazolium bromide (MTT) were purchased from Sigma Aldrich, Germany. Dulbecco's Modified Eagle Medium (DMEM), fetal bovine serum (FBS) and penicillin-streptomycin solution were purchased from Biowest, France.

3.2. SAMPLES PREPARATION

3.2.1. Synthesis of β-Tricalcium Phosphate

β-TCP material was prepared by microwave-assisted wet precipitation method (Motameni et al., 2020). About 42.51 g of $Ca(NO_3)_2 \cdot 4H_2O$ was dissolved in 200 mL of distilled water, forming solution A. 15.85 g of $(NH_4)_2HPO_4$ was dissolved in 200 mL distilled water, forming solution B. The solutions were kept under magnetic stirrer until the powders were completely dissolved in the distilled water. Solution B

was added dropwise under constant stirring to solution A. pH was kept at 7 using ammonium hydroxide. Then, the solution mixture was left under stirring for 30 min at room temperature and transferred to a microwave oven (SAMSUNG, MS23F301EAW). The mixture was heated at 800W for 5 min. The precipitated mixture was filtered and washed with distilled water. Then, dried in an oven set at 80 ºC (Eurotherm) for overnight. Finally, it was calcined at 1000 ºC Protherm PLF 140/5) for 2 h.

3.2.2. Preparation of Sodium Alginate / Dicalcium Phosphate Cement Composites

The pure phase of DCP cement was prepared by mixing 1 g of β-TCP and 1 g of Monocalcium phosphate monohydrate (MCPM) in a mortar. Then, about 1 mL of distilled water was thoroughly mixed with the powder mixture until a homogeneous paste was obtained. SA/DCP cement composites were prepared using the same method except for different amounts of SA were added to 1 mL of water. In Figure 3.1 there is a picture of SA solutions. Amounts of reactants used for DCP and SA/DCP cements preparation are listed in Table 3.1.

Table 3.1. Preparation of cements.

Sample ID	Solid phase		Liquid Phase	
	β-TCP	MCPM	H_2O	SA
DCP	1 g	1 g	1 mL	0.000 g
0.5% SA/DCP	1 g	1 g	1 mL	0.005 g
1.0% SA/DCP	1 g	1 g	1 mL	0.010 g
2.0% SA/DCP	1 g	1 g	1 mL	0.020 g
3.0% SA/DCP	1 g	1 g	1 mL	0.030 g

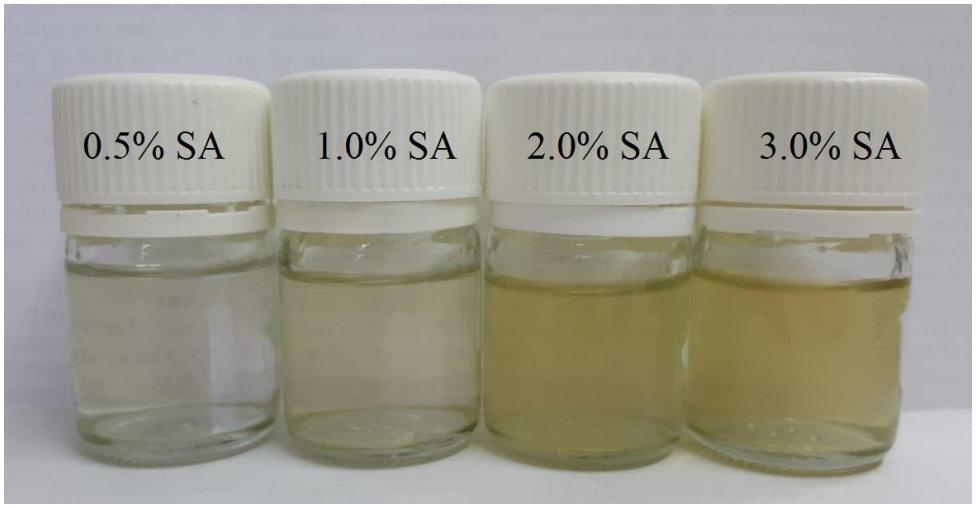

Figure 3.1. SA solutions.

3.3. CHARACTERIZATIONS

3.3.1. X-Ray Diffraction

The phase purity of the prepared materials was investigated using X-ray diffraction (XRD, Rigaku Ultima IV). The samples were scanned from 20º to 80º in 2θ angle and the lattice parameters were calculated using the integrated software package. The phase purity of the entire materials was detected via matching with standard patterns (Joint Committee on Powder Diffraction and Standards (JCPDS)).

3.3.2. Field Emission Scanning Electron Microscopy

Particle size and morphology were analysed using Field emission scanning electron microscopy (FESEM, Carl Zeiss Ultra Plus Gemini). Samples were pre-coated with a gold thin film to reduce the spark rate. Average particle size and particle size distribution were determined by measuring the size of 50 particles selected at random from FESEM images using image analysis software ImageJ (National Institutes of Health, USA).

3.3.3. Inductively Coupled Plasma - Optical Emission Spectrometry

Inductively coupled plasma - optical emission spectrometry (ICP-OES) is a technique used for the detection of chemical elements. This technique was used to detect chemical elements of β-TCP (Perkin Elmer Optima 4300DV). Approximately 500 mg of sample is decomposed overnight in a mixture of 10 mL of concentrated nitric acid (HNO_3) and hydrochloric acid (HCl) at a ratio of 1:3. Then, the solution undergoes several dilutions prior to inject inside analyzing chamber of ICP-OES.

3.3.4. Fourier-Transform Infrared Spectroscopy

Presence of functional groups was confirmed by using Fourier-Transform Infrared Spectroscopy (FTIR, Bruker IFS 66/S) device. All spectra were recorded in transmission mode in the scanning range of 4000-400 cm^{-1}.

3.3.5. Thermogravimetric Analysis

The thermogravimetric analysis (TGA) was carried out under a nitrogen atmosphere (Perkin Elmer Pyris 1) from room temperature to 950 ºC. Depending on the temperature, changes in the sample weights were monitored to study the thermal stability of the prepared materials.

3.4. SETTING TIME

The initial time (IT) and final time (FT) of the cements were measured using a Gillmore needle (ASTM Standard C266-04, 2004). Briefly, about 1 g of the cement paste prepared in Table 3.1 poured in 16 mm diameter and 3 mm height Teflon mould. A needle with a diameter of 2.12 ± 0.05 mm and weight of 113.4 ± 0.5 g was placed on the surface of the cement paste and IT recorded when the needle does not leave any traces on the specimen. Similarly, a needle with a diameter of 1.06 ± 0.05 mm and weight of 453.6 ± 0.5 g was placed on the surface of the cement paste and FT when the needle does not leave any traces on the specimen. The experiments conducted in triplicate and measurements were recorded every 30 sec.

In Figure 3.2 there are pictures of the mould and the Gillmore needle.

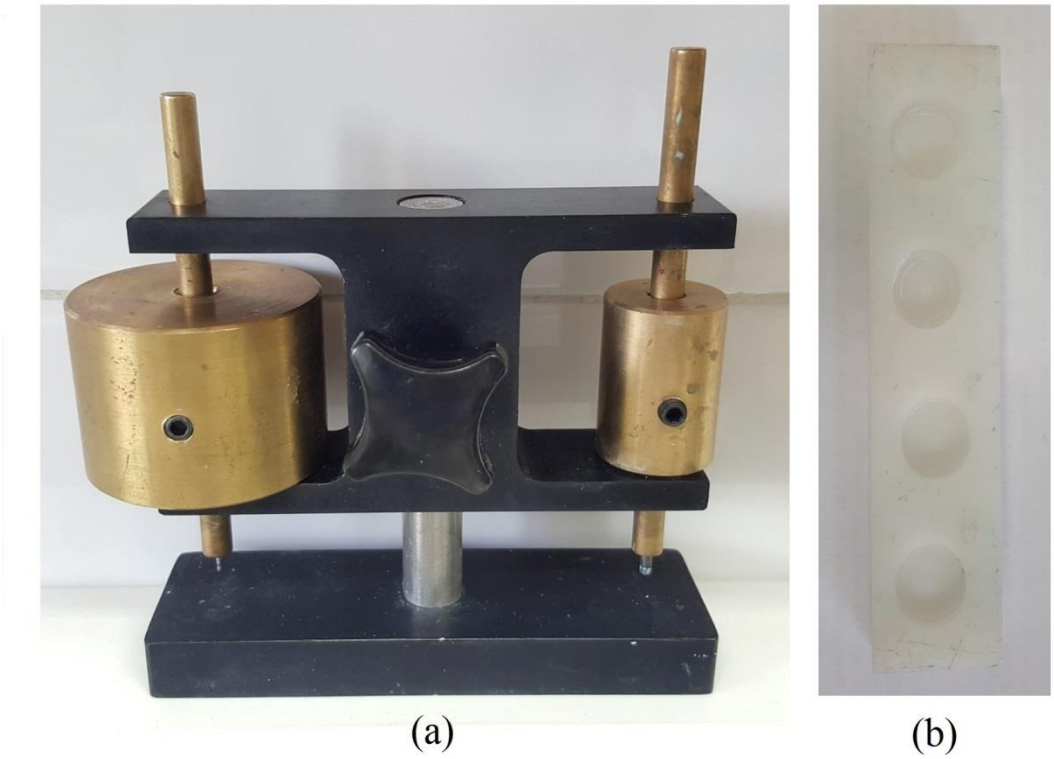

Figure 3.2. a) Gillmore needle and b) the mould for setting time.

3.5. INJECTABILITY TEST

Injectability of the cement paste was investigated utilizing commercial 10 ml syringe sterile similar to the method reported in previous studies (Saleh et. al., 2016 ; Zhou et al., 2015). Briefly, after homogenization, the paste was poured into a commercial syringe with a slit tip 2 mm in diameter. About 5 kg of weight fixed vertically on the top of the plunger for 2 min. The amount of paste before and after injection was quantified and the injectability was determined by the following Equation (3.1). In Figure 3.3 there is a picture of injectability setup.

Figure 3.3. Injectability testing.

$$Inj\% = (W_F - W_A) / (W_F - W_E) \text{ X } 100 \quad (3.1)$$

Where Inj (%) referred to the injectability (%), W_F is the weight of the syringe packed with paste and W_A is the weight of the syringe after injection and W_E is the weight of the empty syringe. The tests were performed in triplicate.

3.6. *IN VITRO* BIODEGRADATION AND MECHANICAL ANALYSIS

3.6.1. Scaffold Shaping

The DCP and SA/DCP paste was poured into a split Teflon mould of 6 mm diameter and 12 mm height and extruded carefully in a disc shape. In Figure 3.4 there are pictures of mould and scaffolds.

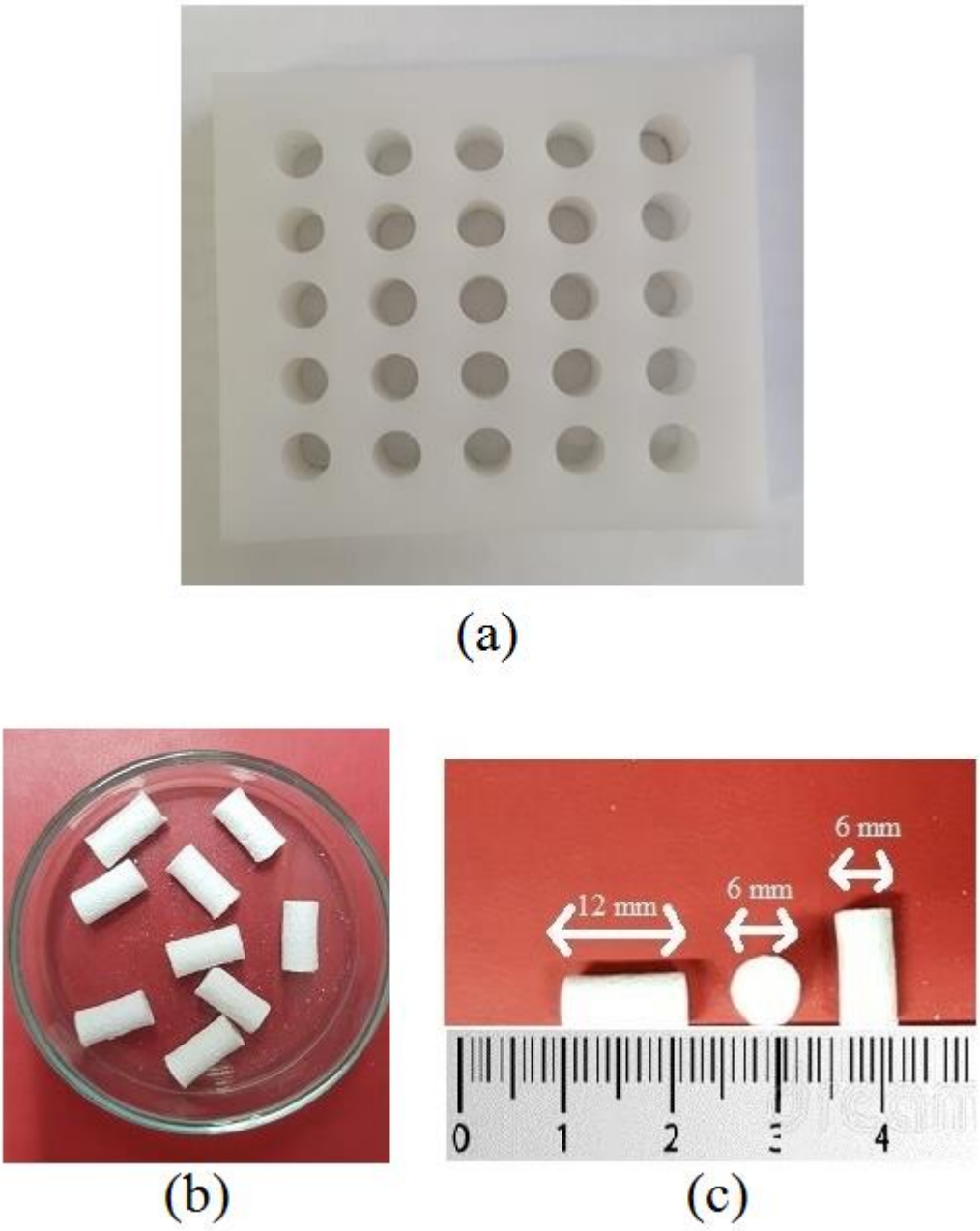

Figure 3.4. a) 6 mm diameter and 12 mm height Teflon mould, b) scaffolds and c) measure of a scaffold.

3.6.2. Preparation of Simulated Body Fluid

In a plastic beaker 480 mL of distilled water was added and the beaker was covered with foil. The solution was mixed in a beaker with a magnetic stirrer and solution temperature was adjusted at 37 ºC. After the temperature reached to 37 ºC, reagents

were added and dissolved one by one in the order as seen in Table 3.2. When the first 9 reagents were added, the pH of the solution was adjusted to 7.4 by adding few drops of HCl (1.0 M). With 480 mL distilled water and 20 mL HCl, a total of 500 mL Simulated Body Fluid (SBF) were obtained.

Table 3.2. Order and amounts of reagents for preparing 500 mL of SBF (Tadashi & Takadama, 2006).

Order	Reagents	Amount
1	NaCl	4.0175g
2	$NaHCO_3$	0.1775g
3	KCl	0.1125g
4	$K_2HPO_4 . 3H_2O$	0.1155g
5	$MgCl_2 . 6H_2O$	0.1555g
6	1.0M–HCl	20mL
7	$CaCl_2$	0.1460g
8	Na_2SO_4	0.0360g
9	Tris(hydroxymethyl)aminomethane	3.059g
10	*1.0M–HCl*	*0-5mL*

The biodegradation of the disc sample was evaluated by SBF. The discs were incubated for 1, 3, 7, 14 and 21 days into 15 mL sterile conical centrifuge tubes (one disc per tube) in shaking water bath at 37 ºC. At each period, the discs were gently removed then rinsed by distilled water followed by absolute ethanol and finally dried at room temperature.

3.6.3. Weight Loss, Density and Porosity

Weight loss, density, and porosity of cements after immersion in SBF for 0, 1, 3, 7, 14 and 21 days were measured. The percentages of weight loss were estimated using Equation 3.2 (Aydogdu et al., 2016).

$$\text{Weight Loss}(\%) = \left(\frac{W_0 - W_f}{W_0}\right) x100 \quad (3.2)$$

Where W_0 referred to the weight of scaffold before the immersion and W_f represents the weight of scaffold after a specific immersion period. The experiments were carried out in triplicates.

The apparent densities of discs of cements were measured by using the Archimedes principle (Equation 3.3).

$$p = \frac{A}{A\text{-}B} p° \quad (3.3)$$

Where p represents the apparent density, A is air-weight, B is water-weight and p^o is the water density (1 g/cm^3).

The total porosity of the materials was calculated using Equation 3.4.

$$\text{Total Porosity } (\%) = \left(\frac{V_{\text{total pore}}}{V_{\text{total}}}\right) x\ 100 \quad (3.4)$$

Where Φ is porosity, m_{dry} is a dry weight of scaffold and m_{wet} is water weight of scaffold.

3.6.4. Compressive Strength Tests

Firstly, samples were immersed in SBF at 37 °C for 0, 1, 3, 7, 14 and 21 days. After each immersion time point in SBF, the cement specimens (6 mm (diameter) x 12 mm (height)) were gently removed and dried at room temperature. The compression strength test was performed using Universal testing systems (Instron 5565A, USA) (ASTM Standard F451-16, 2016). It was applied with a capacity of 5 kN at a 2 mm/min crosshead speed. The tests were performed in triplicates.

3.6.5. *In Vitro* Ca^{2+} Ions Release

The release of Ca^{2+} ions from the cement formulations in SBF was determined at different incubation periods colorimetrically by a stable interaction with o-cresolphthalein complexone. Briefly, about 0.0024 g o-cresolphtalein complexone was dissolved in 10 mL distilled water and mixed thoroughly with a solution of 8-hydroxyquinoline-5-sulfonic acid (0.025 g dissolved in 10 mL distilled water). About 20 ml (0.5 M) of 2-amino-2-methyl-1-propanol was added to the solution mixture, and the colour of the solution turns a purple colour. At each immersion period, 100 µL of aliquot was collected from SBF and mixed with 900 µL (0.1M) HCl for 5 min. Then, 25 µL was taken from the last solution mixture and added to the 120 µL reagent in 96 well plates. After mixing their optical densities were measured at 560 nm by using a microplate spectrophotometer (SpectraMax iD3, USA) (Aydogdu et. al., 2016). The experiments were carried out in triplicates.

3.7. *IN VITRO* CELL CULTURE ANALYSIS

3.7.1. Preparation of Phosphate Buffered Saline

800 mL of distilled water was poured into a beaker to prepare 1 L of Phosphate Buffered Saline (PBS). The solution was mixed with a magnetic stirrer. All the reagent salts (Table 3.3) were dissolved in 800 mL of distilled water. By adding 1.0M-HCl or NaOH, the solution's pH was set to 7.4. Until the volume is 1 L, distilled water was added.

Table 3.3. Amount of the reagents used in the PBS preparation.

Reagents	**Amount**
NaCl	8 g
KCl	0.2 g
Na_2HPO_4	1.44 g
KH_2PO_4	0.24 g
1.0M–HCl	*0-5mL*
NaOH	*0-5 mL*

3.7.2. Cell Culture Tests

The prepared cements were cast in disc shape (6 mm (diameter) x 2 mm (height)) and the mould for producing these discs are shown in Figure 3.5. They were then sterilized by UV irradiation (254 nm) for 1 h for each side of the disc. The discs were rinsed with sterile phosphate-buffered saline (PBS, 0.1M, pH 7.4) for 1 h. This was followed by rinsing with Dulbecco's Modified Eagle Medium (DMEM) supplemented with 10% Fetal bovine serum (FBS) and 1% penicillin-streptomycin solution for 30 min and immersion in complete medium at 37 °C in carbon dioxide incubator for 7 days. After 7 days incubation in complete medium, the discs were gently removed, and the extracts of discs were collected and centrifuged at 14000 rpm for 15 min. The supernatants were collected and stored for future use. Meanwhile, human dental pulp stem cells (DPSCs) from the third molar (isolated and characterized as a stem cell by Rad et. al. (2018)) were sub-cultured for 3 passages. All experiments were performed in four replicates.

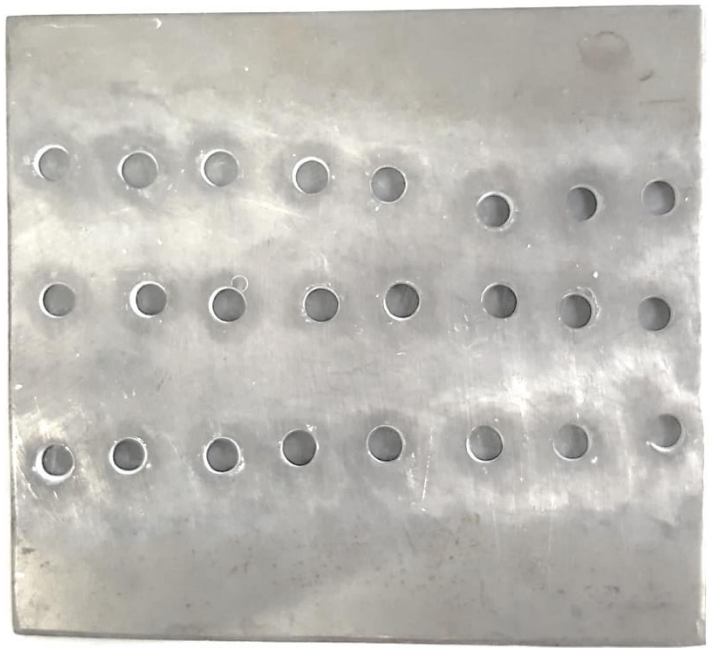

Figure 3.5. The mould for cell culture discs.

3.7.2.1. Cell Viability with MTT

In vitro cytotoxicity effects of the cement's extracts were evaluated via the indirect method by measuring the formation of formazan from MTT (3-[4,5-dimethylthiazole-2-yl]-2,5-diphenyltetrazolium bromide) spectrophotometric.

DPSCs cultured in DMEM supplemented with 10% FBS and 1% penicillin-streptomycin solution. Then DPSCs were seeded in 96-well plates at a density of 2500 cells/well and incubated at 37 °C in a carbon dioxide incubator for overnight. The cell culture media was replaced with cements extracts media (prepared in section 2.7) and the DPSCs incubated with the extract's media for 24 h. After a 24 h incubation period, the extractions medium was discarded, the cells and wells of tissue culture plate were rinsed with sterile PBS. After the rinsing process, about 100 µl of 0.5 mg/mL 1X MTT solution was added to each well, the well plates were covered with aluminium foil and incubated at 37 °C for 4 h. Then, the MTT solution in the wells was discarded and the formazan crystals formed inside cells. The formazan crystals were solubilized in 100 µl of dimethyl sulfoxide by gentle shaking

for 20 min on an orbital shaker in the dark. The supernatants were collected and transferred to a fresh 96-well plate. The absorbance was measured at 570 nm using a microplate reader (SpectraMax iD3, USA). The DPSCs were incubated in untreated cell culture media used as a control group.

To calculate the percentage of cell viability, for background control (negative controls) optical densities are averaged. This value is subtracted from all values. For control (*healthy cells with 100% viability*) average was calculated. Each value divided by control and multiplied by 100 ((value / control) * 100). This value is the percentage of cell viability. Then, the same group's values were averaged and the standard deviation was calculated.

3.7.2.2. Cell Fixation

100 mL PBS was put in a beaker and heated to 60 ºC with magnetic stirrer. Then 4 g paraformaldehyde powders were added to the heated PBS and waited for dissolving. Beaker was covered with foil to protect from the light.

DPSCs were cultured and grown in DMEM. Cells were trypsinized and collected by centrifugation at 2000 rpm for 5 min at room temperature. Then cells were counted by using a hemocytometer. $5x10^4$ DPSCs were seeded on 48 well plates, 500 µl DMEM low glucose with 10% FBS and 1% penicillin-streptomycin was put on wells and the cells were incubated at 37 ºC and 5% CO_2 for 24 h.

After 24 h mediums in wells were removed and washed with 500 µl PBS in dark. 500 µl paraformaldehyde solution was added to each well and waited 20 min at room temperature. After 20 min paraformaldehyde solution was removed and 500 µl PBS was added to each well. After 5 min PBS was removed and 500 µl PBS was added again.

3.7.2.3. Cell Morphology Examination

The DPSCs were seeded on cover glasses at a cell density of 5000 cells/glass and cultured in complete medium for 24 h. After a 24 h incubation period, the cell culture media was replaced with extraction media and incubated for 24 h. At the end of the incubation period, the cells were fixed with 4% (w/v) paraformaldehyde solution for 15 min at 37 °C. Afterwards, the paraformaldehyde solution was discarded and cells were washed with PBS. Then, the cell membranes were permeabilized with 1% (v/v) Triton X-100 in PBS for 5 min at room temperature. After washing with PBS, cells were incubated in 1% (w/v) of bovine serum albumin (BSA) solution in PBS for 1 h at 37 °C. Then, to stain actin filaments, cells were incubated with Alexa flour 488 phalloidin in 0.1% (w/v) of BSA in PBS for 1 h at 37 °C. After washing with 0.1% (w/v) of BSA in PBS, to stain cell nuclei, cells were incubated with DAPI (4′,6-diamidino-2-phenylindole) in 0.1% (w/v) of BSA in PBS for 10 min at room temperature. After washing with PBS, cell morphology was assessed with Zeiss Axio Scope A1 (Zeiss, Germany) under fluorescence of excitation at 488 nm for Alexa flour (green) and 350 nm for DAPI (blue).

3.7.2.4. Statistical Analysis

All experiments were performed with n=3, except for MTT analysis. MTT analysis was replicated with n=4. All data are demonstrated as mean ± standard deviation. Results were analysed using a one-way analysis of variance (ANOVA) and Tukey's multiple comparison test.

CHAPTER 4

RESULTS AND DISCUSSION

4.1. CHARACTERIZATION OF β-TCP

The XRD pattern of β-TCP powder is illustrated in Figure 4.1. All diffraction peaks of the prepared β-TCP were in good match with the standard phase of β-TCP (whitlockite phase, JCPDS 09–0169). No other CPs phases were observed. Particularly, no peak was detected at 32.196º, indicating that the synthesized powder existed as single-phase and no HA phase (JCPDS 09–432) was present.

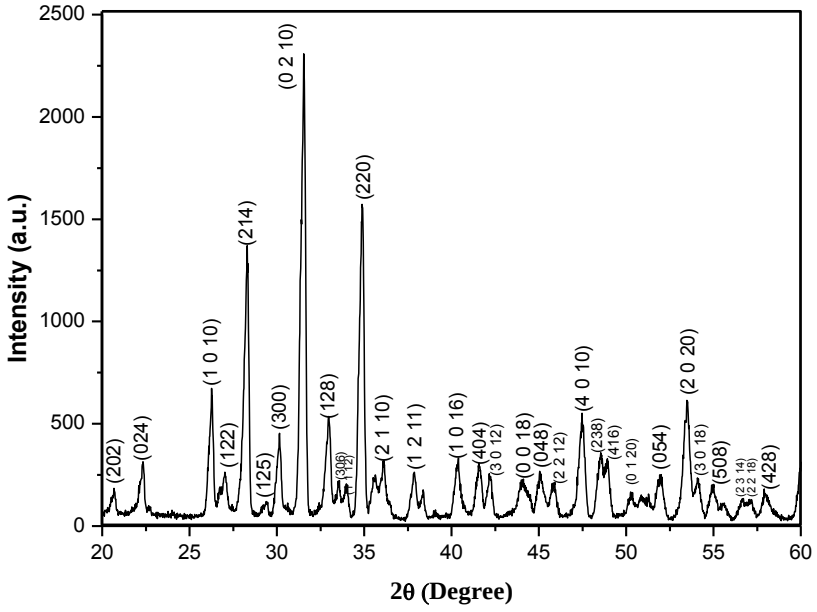

Figure 4.1. XRD pattern of β-TCP calcined at 1000 ºC for 2 h.

SEM micrograph of β-TCP powder is shown in Figure 4.2. β-TCP particles appeared in globular shape with rounded edges, the particles coalesced due to heat-treatment at high temperature. However, similar observations were reported in previous studies (Mirhadi et al., 2011; Grigoraviciute-Puroniene et al., 2017; Taha et al., 2017). Particle distribution was plotted based on diameters of 50 particles and the results are ascribed in Figure 4.2. Average particle size was about 1000 nm (1 µm). Mirhadi et al., (2011) synthesized β-TCP particles using a wet chemical process, followed by calcination at 700 ºC for 2 h. The average size of the obtained particles was about 150 nm. Grigoraviciute-Puroniene et al., (2017) synthesized β-TCP particles using wet precipitation method and they calcined at 800 °C for 5 h. The group reported that the average size of the obtained particles was about 150 nm. However, in this thesis, the average size of the prepared particles was bigger than those reported in previous studies. This could be attributed to high particle growth rate during heat treatment. Ca/P ratio was found 1.39, which was slightly lower than the desired value (1.5).

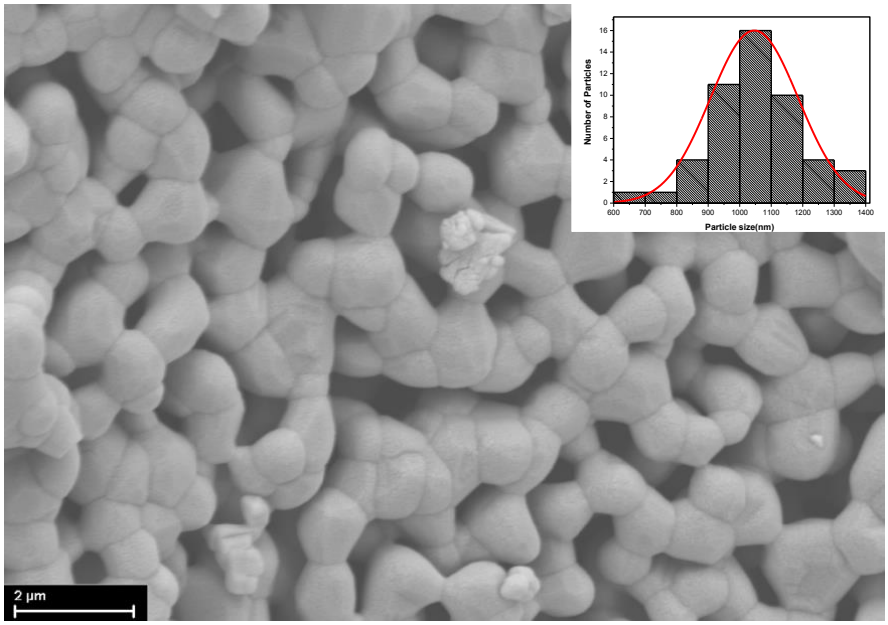

Figure 4.2. FESEM image and particle distributions of β-TCP sample calcined at 1000 ºC for 2 h.

FTIR spectra of β-TCP powder are shown in Figure 4.3 and characteristic peaks of β-TCP in the FTIR spectrum were shown in Table 4.1. The bands at 431 and 496 cm^{-1} belong to the υ2 mode of PO_4^{3-}. The bands at 542 cm^{-1}, 589 cm^{-1} and 604 cm^{-1} were assigned to the vibration mode of PO_4^{3-} (υ4). The bands located in between 943 cm^{-1}

and 1214 cm^{-1} were attributed to the υ1 (symmetric stretching) and υ3 (asymmetric stretching) mode of PO_4^{3-} group. Locations and shapes of the peaks were well matched with FTIR results of previous studies (Raynaud et al., 2002; Chen et al., 2008). Stretching and bending bands corresponding to hydroxyl (-OH) groups were not detected at 630 cm^{-1} and 3570 cm^{-1} confirming synthesis of single-phase β-TCP. The peak at 727 cm^{-1} showed the presence of $P_2O_7^{4-}$ ions which belongs to one of the β-TCP precursors [β-calcium pyrophosphate (β-$Ca_2P_2O_7$)]. This peak becomes sharper which confirms the conversion of HPO_4^{2-} to β-TCP after calcination at 1000 °C (Abdel-Fattah et al., 2008).

Table 4.1. Characteristic peaks of β-TCP in the FTIR spectrum.

Peak Number	Wavelength (cm^{-1})	Band Assignment
1	431	PO_4^{3-} mode (υ2)
2	496	PO_4^{3-} mode (υ2)
3	542	PO_4^{3-} vibration mode (υ4)
4	589	PO_4^{3-} vibration mode (υ4)
5	604	PO_4^{3-} vibration mode (υ4)
6	727	$P_2O_7^{4-}$ ions
7	943	PO_4^{3-} symmetric stretching mode (υ1)
8	970	PO_4^{3-} symmetric stretching mode (υ1)
9	1002	PO_4^{3-} asymmetric stretching mode (υ3)
10	1101	PO_4^{3-} asymmetric stretching mode (υ3)
11	1157	PO_4^{3-} asymmetric stretching mode (υ3)
12	1190	PO_4^{3-} asymmetric stretching mode (υ3)
13	1214	PO_4^{3-} asymmetric stretching mode (υ3)

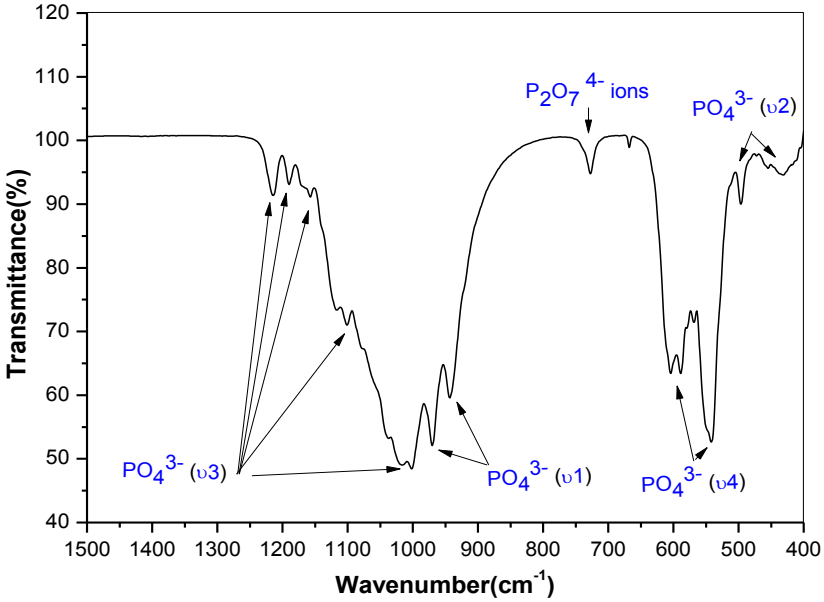

Figure 4.3. FTIR pattern of β-TCP calcined at 1000 ºC for 2 h.

4.2. CHARACTERIZATION OF PURE DCP AND SA/DCP

XRD patterns of pure DCP and SA/DCP self-hardened at room temperature are illustrated in Figure 4.4. Diffraction peaks of DCP were in good match with a standard phase of monetite (JCPDS 71-1760). No peak was detected at 20.95º, indicating that prepared DCP existed as single-phase (Monetite), and brushite phase (JCDPS 72-1240) was absent. With incorporation of SA into DCP, no change in peaks intensity and shape was observed. Furthermore, a small increase in lattice parameters (a, b and c) was detected (Table 4.2). This expansion in lattice parameter could be due to the ionic exchange that took place between Na^{+} ions of SA and a part of Ca^{2+} of DCP, whereas Ca^{2+} ions are used for crosslinking of SA.

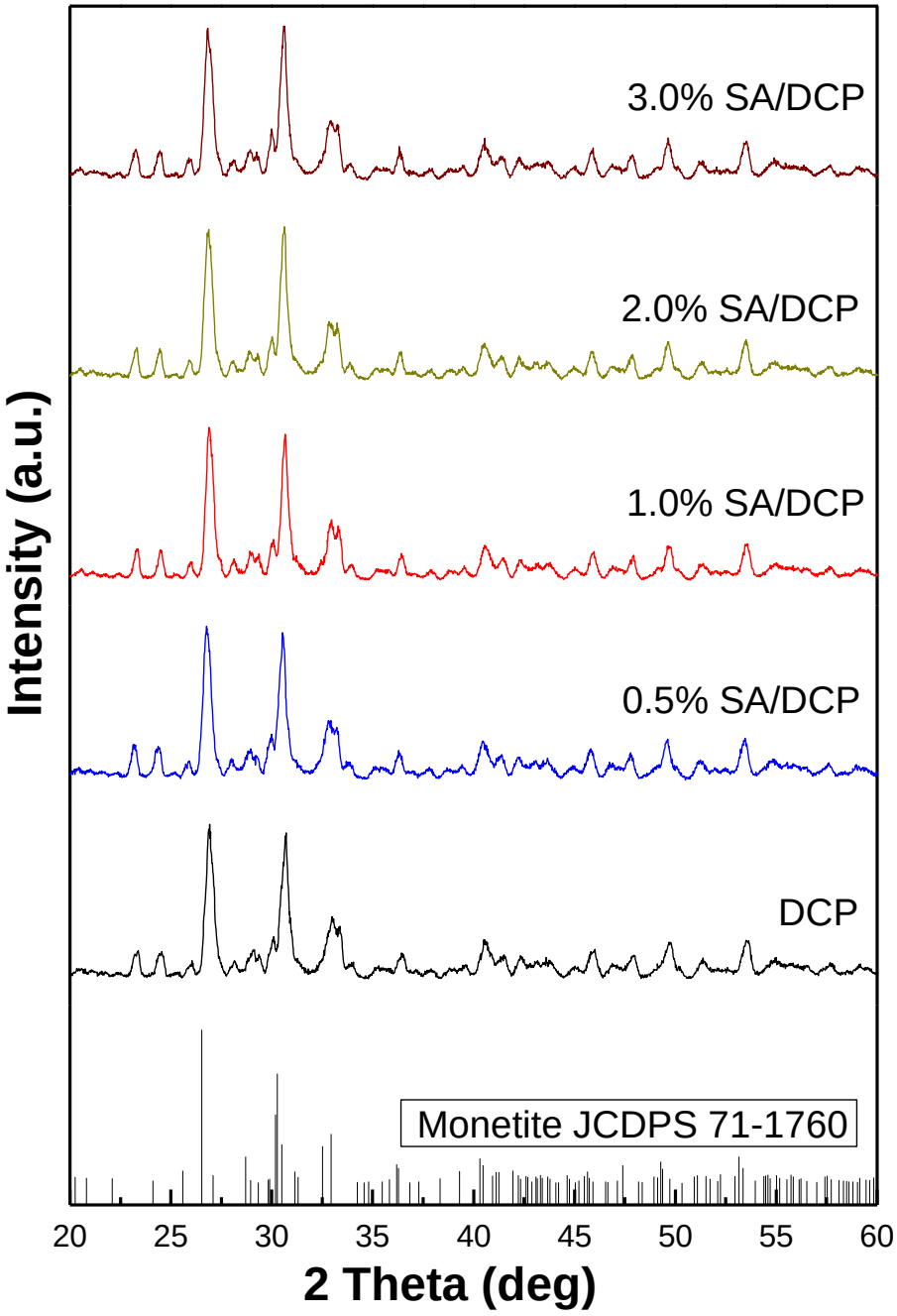

Figure 4.4. XRD patterns of pure DCP and SA/DCP cement composites.

Table 4.2. Lattice parameters of pure DCP and SA/DCP cement composites.

Sample ID	**Lattice Parameters**			
	***a*(Å)**	***b*(Å)**	***c*(Å)**	**V(Å)^3**
Monetite	6.916	6.619	6.946	307.000
DCP	6.853	6.559	6.883	298.714
0.5% SA/DCP	6.889	6.594	6.919	303.445
1.0% SA/DCP	6.887	6.594	6.956	304.810
2.0% SA/DCP	6.860	6.566	6.890	299.611
3.0% SA/DCP	6.873	6.578	6.903	301.324

Micrograph images of pure DCP and SA/DCP set at room temperature are displayed in Figure 4.5. FESEM examinations showed that pure DCP particles had a large irregular plate-like structure with an average width ranging from micro to nanometer dimensions. This fluctuation in plate dimensions could be assigned to different degrees of agglomerations. However, a similar observation was reported by other researchers (Tas, 2009; Sridhar, 2010). Addition of SA resulted in the inhibition of growth of different forms of crystals with no clear changes in particle shape.

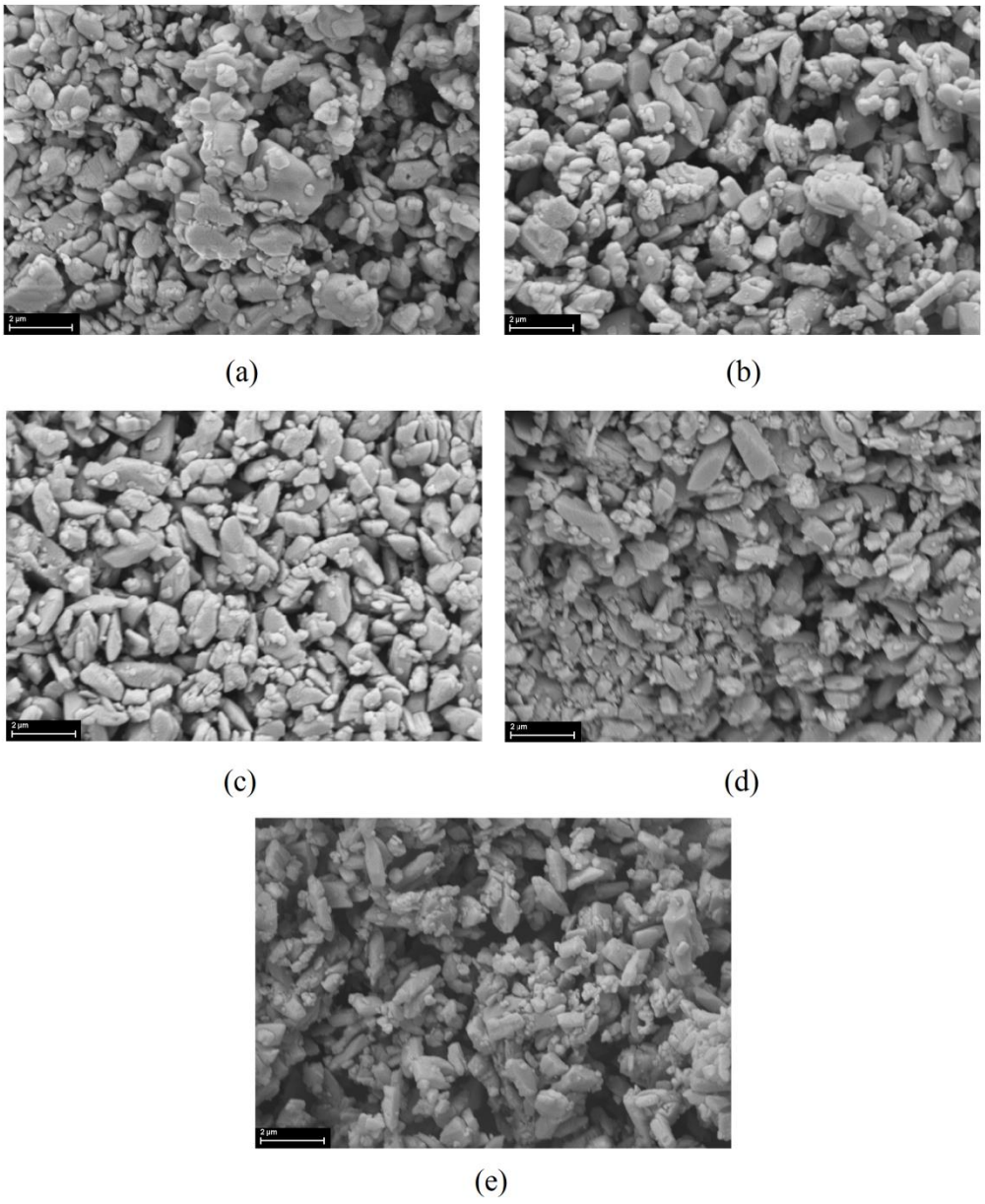

Figure 4.5. SEM images of a) DCP, b) 0.5% SA/DCP, c) 1.0% SA/DCP, d) 2.0% SA/DCP, e) 3.0% SA/DCP cement composites. Scale bar is 2µm.

FTIR spectra of pure DCP and SA/DCP are shown in Figure 4.6 and characteristic peaks of cements in the FTIR spectrum are shown in Table 4.3. The representative peaks existed in narrower shape, indicating structural distortion due to the existence of excess SA. Two peaks were located at 523 cm^{-1} and 558 cm^{-1} were ascribed to the stretching mode of P-O-H of the HPO_4^{2-}. A single peak was detected at 887 cm^{-1} was assigned to the bending mode of P-O. The broadband was determined within the 975 cm^{-1} - 1128 cm^{-1} range was attributed to the stretching mode of P-O. Another peak

was observed at 1350 cm^{-1} was attributed to the bending mode of P-O-H. Furthermore, the broadband was observed at 1642 cm^{-1} which was ascribed to H-O-H bending and rotation of the residual free water (Mhla & Koutsoukos, 2017).

Table 4.3. Characteristic peaks of cements in the FTIR spectrum.

Peak Number	Wavelength (cm^{-1})	Band Assignment
1	523	P-O-H stretching mode of the HPO_4^{2-}
2	558	P-O-H stretching mode of the HPO_4^{2-}
3	887	P-O bending mode of the HPO_4^{2-}
4	975	P-O stretching mode of the HPO_4^{2-}
5	1061	P-O stretching mode of the HPO_4^{2-}
6	1128	P-O stretching mode of the HPO_4^{2-}
7	1350	P-O-H in-plane bending mode of the HPO_4^{2-}
8	1642	H-O-H bending mode

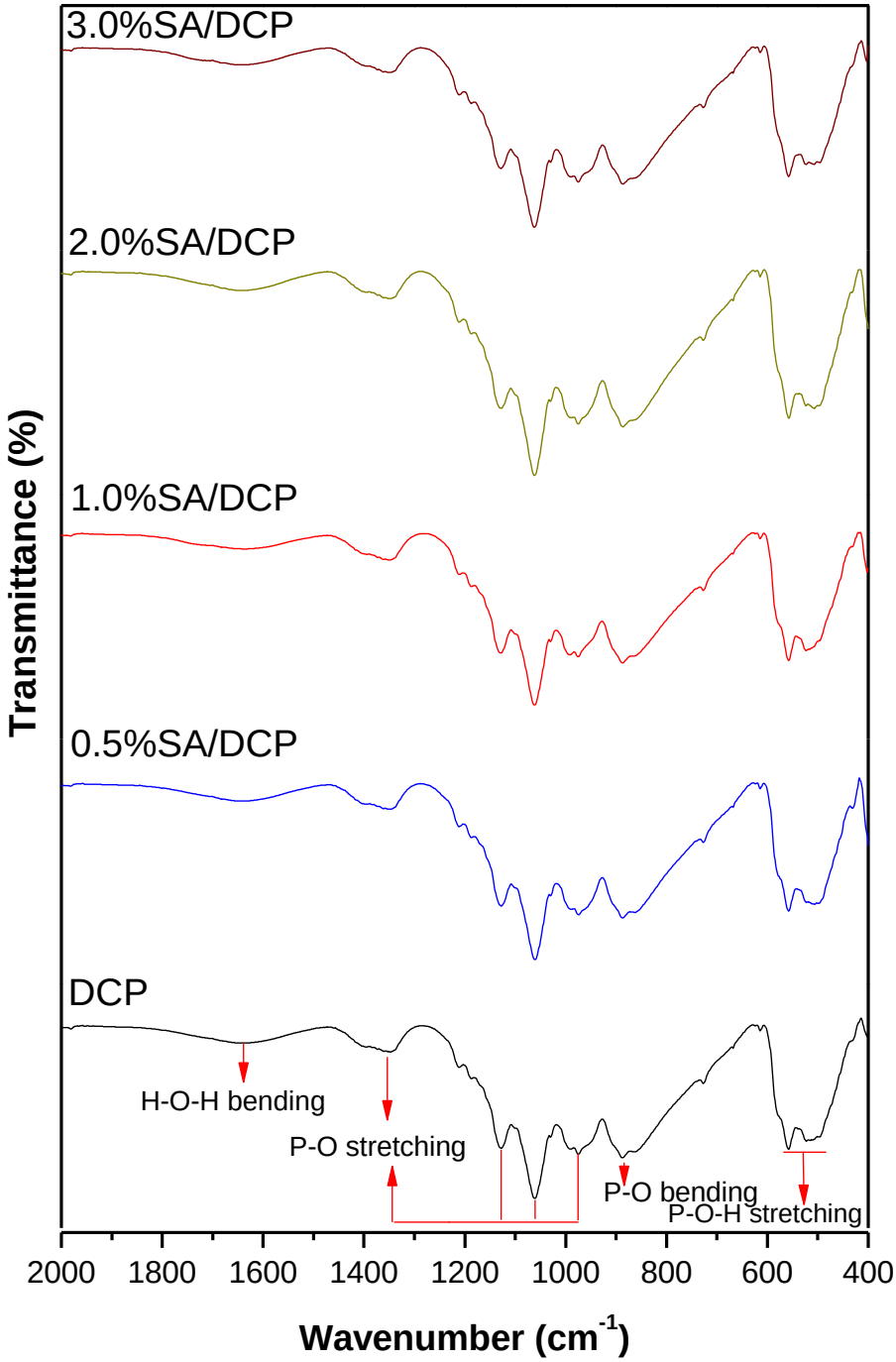

Figure 4.6. FTIR patterns of pure DCP and SA/DCP cement composites.

It was difficult to be detected using XRD, SEM and FTIR techniques because of low SA content of the cements. TGA analysis was conducted to study thermal properties and composition of the cements (Figure 4.7). TGA curves of the crystals consist of four regions (a) 30 °C - 100 °C, assigning to the removal of adsorbed water from the surface of samples, (b) 100 °C - 250 °C, corresponding to the removal of lattice

water (Liao et al., 1999), (c) 250 °C - 400 °C, in this stage of heating two $CaHPO_4$ molecules combine and result in the decomposition that happens with the removal of water molecules, contributing to calcium pyrophosphate formation ($Ca_2P_2O_7$) as shown in Equation 4.1 (Suryawanshi & Chaudhari, 2014).

$$2CaHPO_4 \longrightarrow Ca_2P_2O_7 + H_2O \quad (4.1)$$

Furthermore, in the case of SA/DCP samples this stage was shifted a bit to the higher degree about 450 °C could be attributed degradation and decomposition of SA matrix to carbonate materials like $CaCO_3$ (Dabiri et al., 2016) and (d) 450 °C – 950 °C neglected weight loss was detected, showing that all samples showed thermal stability to a temperature ≥ 450 °C. Total weight losses of pure DCP, 0.5% SA/DCP, 1.0% SA/DCP, 2.0% SA/DCP and 3.0% SA/DCP were 19.6%, 21.42%, 28.64%, 31.77% and 35.38%, respectively. 3.0% SA/DCP showed low thermal stability due to the presence of highest SA amount among others.

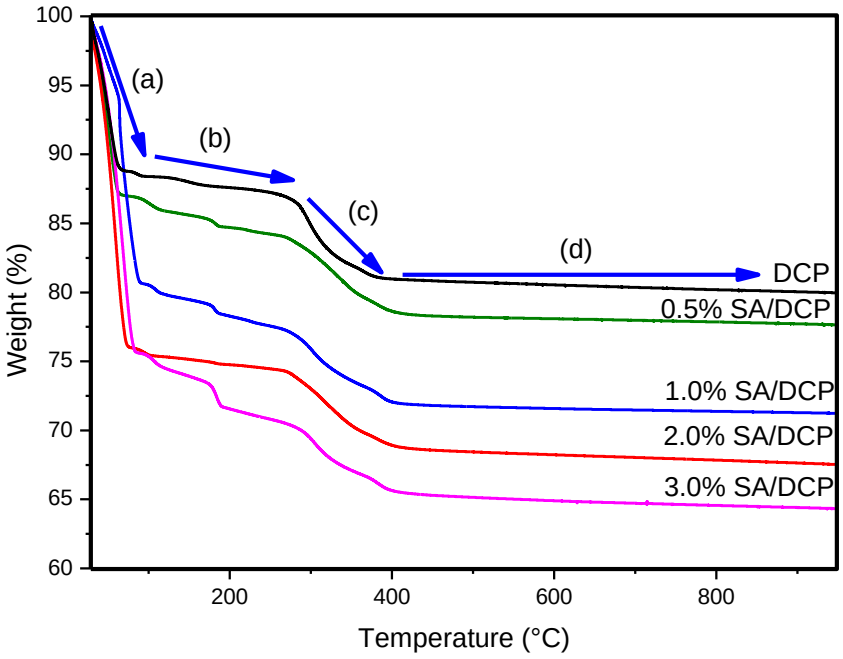

Figure 4.7. Thermograms of pure DCP and SA/DCP cement composites.

4.3. SETTING TIME AND INJECTABILITY MEASUREMENTS

The initial (IT) and final (FT) setting times of pure DCP and SA/DCP were evaluated employing a Gillmore needle at room temperature and the results are shown in Figure 4.8 (a). IT and FT of pure DCP were about 0.6±0.1 min and 7±1 min, respectively, which were close to the values reported in the previous studies (Huan & Chang, 2009; Taha et al., 2017; Luo et al., 2018). The addition of SA caused a significant rise in the setting time of DCP. The setting time of pure DCP raised to more than 7 times when 3.0% of SA was added to the liquid phase. DCP crystals formation by calcium and phosphate ions in water was diffusion controlled. The diffusion rate decreased, as the medium viscosity increased. SA significantly boosted the viscosity by forming viscous sol in aqueous media. Calcium alginate gel formation can play a major inhibitory role in DCP setting. SA sol in the presence of calcium ion is thought to form water-insoluble calcium alginate gel (Ishikawa et al., 1997) as shown in Equation (4.2).

$$2\text{Na-Alg} + Ca^{2+} \longrightarrow CaAlg_2 + 2Na^{+} \quad (4.2)$$

The injectability measurements of the prepared cement compositions were performed at room temperature and the results are shown in Figure 4.8 (b). Injectability of pure DCP was about 82.97±1.55%. The injectability percentage significantly boosted with increasing SA content of DCP and it was about 95.38±2.49% for 3.0% SA/DCP. This behaviour could be related to the viscosity nature of the prepared cements. Ishikawa et al. reported that the addition of SA increased viscosity nature of DCP (Ishikawa et al., 1997). SA/DCP were found to be easy to handle (Figure 4.8 (c)) and they could be used to fill irregular gaps in a bone.

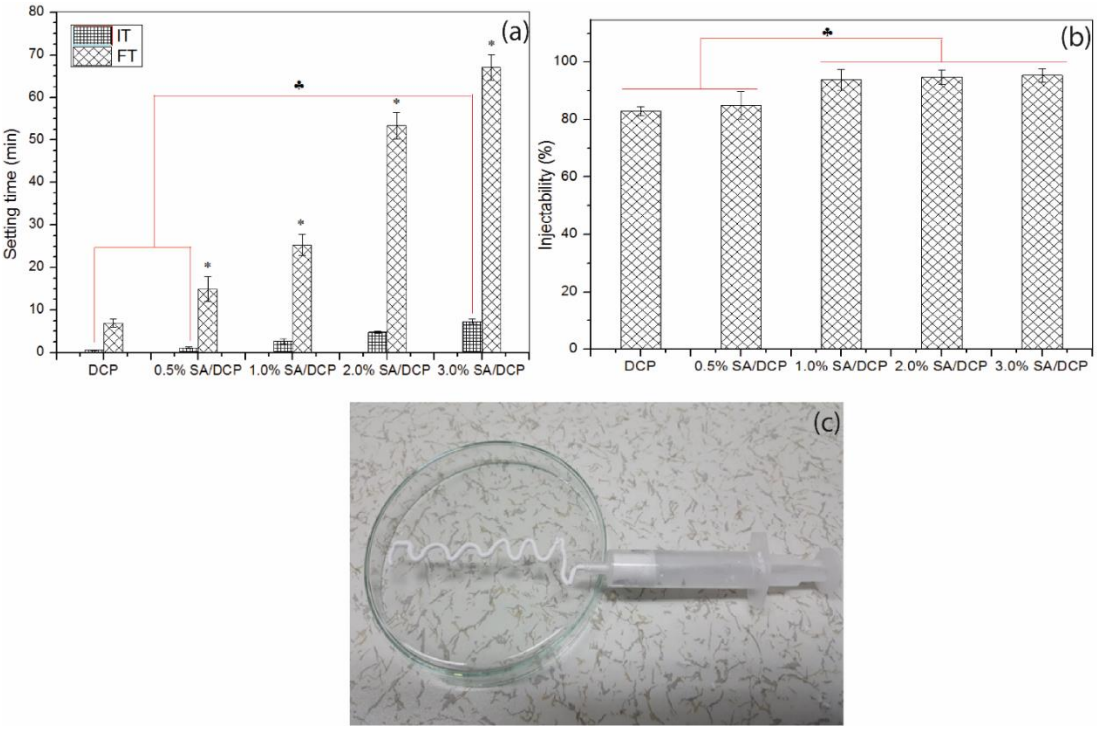

Figure 4.8. a) Initial (IT) and final (FT) setting times, b) %injectability of pure DCP and SA/DCP cement composites and (c) digital image showing the injectability of 3.0% SA/DCP cement composites. Values are given as mean ± standard deviation (n =3); $p^{*} < 0.05$ and $p^{\clubsuit} < 0.05$ denote statistically significant difference between groups.

4.4. *IN VITRO* DISSOLUTION ANALYSIS

Results of cumulative weight loss, density, porosity and Ca^{2+} ion leaching from pure DCP and SA/DCP discs immersed in SBF for 21 days are summarized in Table 4.4. After 1-3 days of incubation in SBF, no significant difference was observed between groups. However, it can be seen the cumulative weight loss of pure DCP discs was higher than that of SA/DCP. Initially, SA as a hydrogel absorbed some amount of water which was then followed by a low weight loss. The weight loss in 3.0% SA/DCP was significantly higher than the other groups between days 7 and 14 and after 21 days of incubation, the weight loss in 2.0% SA/DCP and 3.0% SA/DCP groups was significantly higher than observed in other groups for all days. This could be attributed to the dissolution of SA in SBF (Shahriari et al., 2016).

The density of the cement discs was determined. During 21 days of incubation only at day 3 the density of DCP discs was significantly higher than 3.0% SA/DCP discs.

In general, the lowest density was recorded at 7^{th} day of immersion in SBF for all groups indicating a maximum degradation rate. After 7 days of incubation, an increase in the density was observed, which could be attributed to precipitation of apatite granules.

Porosity percentage of cement scaffolds set at room temperature was calculated, during 1-3 days of incubation, in general, the porosity (%) increased as the SA amount was increased. This could be due to a higher degradation rate of SA/DCP than pure DCP. During the prolonged incubation period, the porosity values fluctuated with addition of SA, no clear trend was observed. This phenomenon could be related to deposition different fractions of apatite particles which could block some pores. However, over 21 days immersion, 3.0% SA/DCP showed slightly higher porosity than pure DCP. Usually, high porosity matrix considered as a good host for adhesion and proliferation of bone cells and then promotes bone tissue regeneration (Jin et al., 2012).

Release of Ca^{2+} ions from scaffolds in SBF over 21 days was measured. For the period 1-3 days, it was observed that the Ca^{2+} ion released in SBF was similar (non-significance was showed), this behaviour could be related to hard surface nature of scaffolds. The maximum amount of Ca^{2+} ions was released in SBF after 7 days of immersion, showing the initiation of the samples surface level dissolution. The amount of Ca^{2+} ions released from 0.5% SA/DCP was significantly higher than 2.0% SA/DCP and 3.0% SA/DCP groups. After 14 days, the amount of Ca^{2+} ions significantly declined for all groups which could be due to the consumption of Ca^{2+} ions in apatite layer formation. Between 14 and 21 days, the concentration of Ca^{2+} was relatively constant, suggesting that the balance between deposition and dissolution was achieved.

Table 4.4. Cumulative weight loss, density, and porosity of DCP and SA / DCP scaffolds immersed in SBF for 1, 3, 7, 14 and 21 days and release of Ca^{2+} ions.

Immersion Time (Day)	Sample ID	Cumulative Weight loss (%)	Density (g/cm^3)	Porosity (%)	Ca^{2+} ions released (ppm)
1	DCP	6.16±0.20	2.38±0.03	21.40±1.36	287.45±23.40
	0.5% SA/DCP	5.46±0.20	2.30±0.01	22.45±0.37	462.72±33.89
	1.0% SA/DCP	5.35±0.52	2.31±0.04	23.38±0.34	439.32±71.96
	2.0% SA/DCP	5.40±0.54	2.22±0.10	24.50±0.83	474.42±193.03
	3.0% SA/DCP	3.37±0.77	2.21±0.03	26.09±0.21	494.15±110.86
3	DCP	6.46±0.94	2.41±0.01♣	20.40±0.08	253.04±9.370
	0.5% SA/DCP	4.63±0.38	2.34±0.18	22.33±1.48	372.56±119.79
	1.0% SA/DCP	5.30±0.45	2.33±0.02	24.12±1.75	402.16±130.55
	2.0% SA/DCP	6.01±0.81	2.18±0.10	25.94±1.95	501.72±184.52
	3.0% SA/DCP	4.72±0.33	2.07±0.09	25.69±1.97	488.41±107.86
7	DCP	15.68±0.41	2.21±0.03	30.82±0.38	643.73±68.42
	0.5% SA/DCP	15.03±0.39	2.20±0.05	28.76±3.89	717.14±39.79▲
	1.0% SA/DCP	15.42±0.95	2.23±0.07	34.04±5.07	652.67±55.20
	2.0% SA/DCP	16.23±0.74	2.24±0.19	28.77±0.69	615.74±99.24
	3.0% SA/DCP	20.37±0.33*	2.17±0.09	30.53±7.19	621.01±81.26
14	DCP	16.13±1.68	2.22±0.03	33.33±1.45	274.60±172.66
	0.5% SA/DCP	16.56±0.83	2.25±0.03	27.62±1.49	457.67±34.02
	1.0% SA/DCP	13.68±1.08	2.23±0.13	32.94±2.02	359.49±118.61
	2.0% SA/DCP	16.60±0.39	2.30±0.11	29.05±2.08	369.58±99.77
	3.0% SA/DCP	20.49±0.56*	2.31±0.15	30.56±2.15	313.83±125.62
21	DCP	15.81±0.69	2.35±0.06	26.58±1.05	437.49±76.21
	0.5% SA/DCP	20.32±3.22	2.34±0.01	24.71±2.10	528.91±198.07
	1.0% SA/DCP	17.19±1.51	2.43±0.03	30.67±3.71	478.09±173.69
	2.0% SA/DCP	27.49±1.70*	2.21±0.06	26.31±1.56	516.86±27.24
	3.0% SA/DCP	23.91±0.25*	2.36±0.12	31.65±1.12	483.14±71.08

Values are means ± standard deviation (n =3); $p^* < 0.05$, $p^{\clubsuit} < 0.05$, and $p^{\blacktriangle} < 0.05$ denote the significantly different group at the given time point.

4.5. COMPRESSIVE STRENGTH RESULTS

Mechanical properties of biocements are very important for clinical applications. CP cements are known to have poor mechanical materials and addition of polymeric materials is a common method to enhance the mechanical properties of materials (An et al., 2016). Compressive strengths of pure DCP and SA/DCP scaffolds before and after immersion in SBF for 21 days are illustrated in Figure 4.9. Before soaking in

SBF, the compressive strength of pure DCP scaffold was about 8.5 MPa. As the concentration of SA was increased, the strength of the cement also increased by displaying a non-linear compressive behaviour. However, it significantly increased. This improvement could be due to the crosslinking reaction between the carboxyl group of SA and Ca^{2+} ions on adjacent polymer chains (Bt Ibrahim et al., 2019; Gholizadeh et al., 2018). After immersion in SBF for the period between 1-3 days, the compressive strength increased and this could be assigned to crosslinking of SA, low degradation rate and apatite formation. At the 7^{th} day of incubation, compressive strength significantly decreased for all samples, this behaviour could be attributed to the highest degradation rate. This was in agreement with Ca^{2+} ion releasing profile, which might due to degradation of SA phase. No significant changes were observed on the 14^{th} day of incubation. While, 21^{th} day, compressive strength values increased which might be due to precipitation of apatite particles and a decrease in porosity leading to an increase in compressive strength (see Table 4.4). The outcomes of compressive strength were in good match with accumulative weight loss and porosity results.

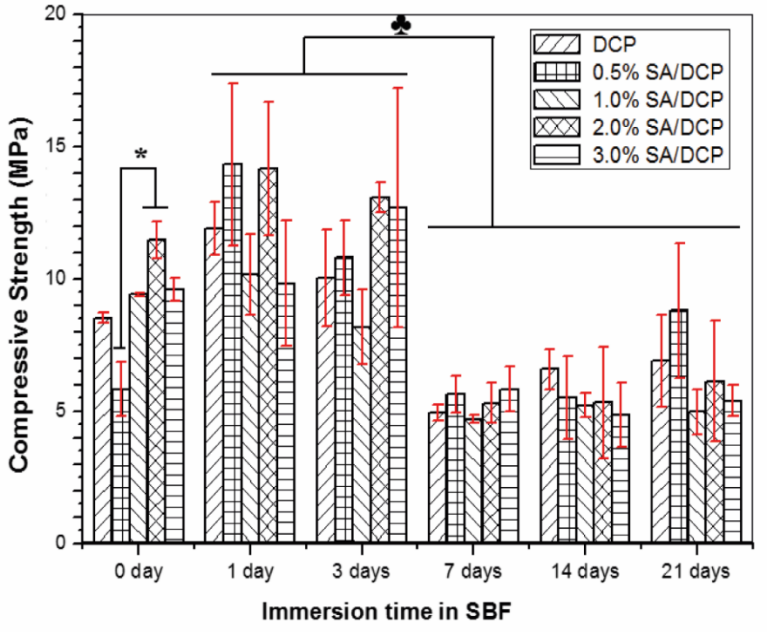

Figure 4.9. Compressive strengths of pure DCP and SA/DCP scaffolds, before and after immersion in SBF for 21 days. Values are given as mean ± standard deviation (n =3); $p^{*} < 0.05$ and $p^{\clubsuit} < 0.05$ denote statistically significant difference between groups.

4.6. CELL VIABILITY AND CELL MORPHOLOGY RESULTS

Viability of DPSCs after 24 h incubation in the extraction media of DCP and SA/DCP is shown in Figure 4.10. Viability of DPSCs incubated in extracts of cements was significantly higher than that of the control group. Results showed that all cements were cytocompatible. Cell viability in 0.5% SA/DCP was significantly the highest among groups while cell viability of the control was significantly the lowest among groups. Cell viability of 3.0% SA/DCP was significantly lower than all groups except for the control group. On the other hand, there was no significant difference in the cell viability between DCP and 1.0% and 2.0% SA/DCP groups. This means that a minimal amount of SA into DCP scaffold caused a significant increase in cell viability. These results are also compatible with Ca^{2+} ion release from cements after 7 days (see Table 4.4). After 7 days of incubation, Ca^{2+} ion release from 0.5% SA/DCP group was the highest among groups which showed that higher Ca^{2+} ion amount could result in higher cell viability. This result is also in agreement with the literature. Lee et al. (2018) cultivated mouse bone marrow mesenchymal stem cells with cell culture media that contained different concentrations of Ca^{2+} ions and observed that higher Ca^{2+} ion amounts resulted in higher cell viability and elevated levels of cell growth factors such as fibroblast growth factor-2 (FGF2) and transforming growth factor- β1 (TGFβ1).

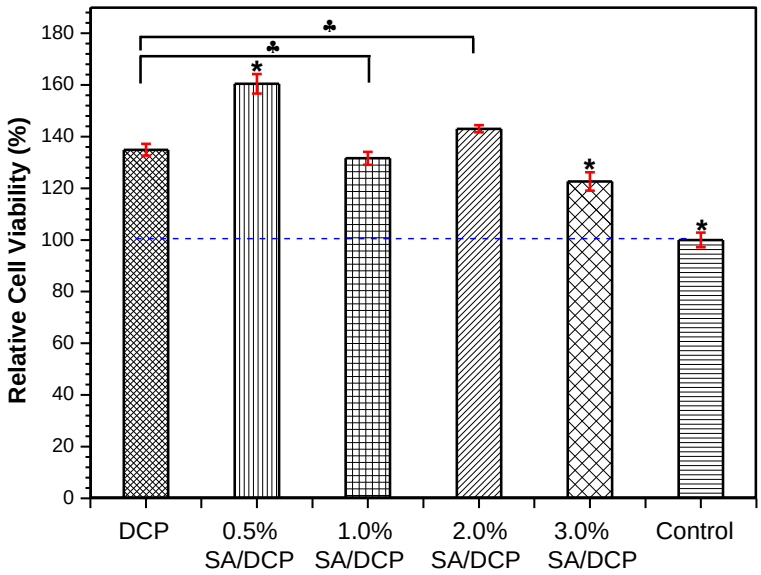

Figure 4.10. Viability of DPSCs after 24 h of incubation with the extraction media of cement discs (n=4). Viability of cells cultured with cell culture media was taken as 100% viable. A significant difference is shown with "*" ($p<0.05$) and the non-significant difference is shown with "♣" $p>0.05$.

Fluorescence microscopy images of DPSCs are shown in Figure 4.11. After 1 day of incubation, cell morphology was fibroblast-like in the control group. However, DPSCs cultured with extraction media of DCP appeared in different shapes. Cells became less spread compared to those cells in control and SA/DCP groups. With the addition of SA, more cell adhesion, spreading, and cell-cell interactions compared to DCP group were observed. Lee et al. (2011) prepared CP cements containing 2.0% of SA, rat bone marrow stromal cells were used to assess cell viability, deduced that addition of SA improved cell viability and cell attachment. Castilho et al. (2015) fabricated 3D printed TCP scaffolds containing 2.5% of SA, used osteoblastic cells (MG63) line as a model to evaluate the cytotoxicity behaviour, demonstrated that addition of 2.5% of SA increased cell viability and cell attachment when compared to pure TCP scaffolds. Wang et al. (2016a) prepared induced pluripotent stem cells-derived mesenchymal stem cells encapsulated alginate microbeads and these microbeads were incorporated into the CP paste. Pure CP paste and microbeads-CP pastes were implanted into nude rats and no signs of inflammation or teratoma formation were observed in all groups. However, cell encapsulated microbeads containing CP paste increased newly formed bone area when compared to pure CP paste.

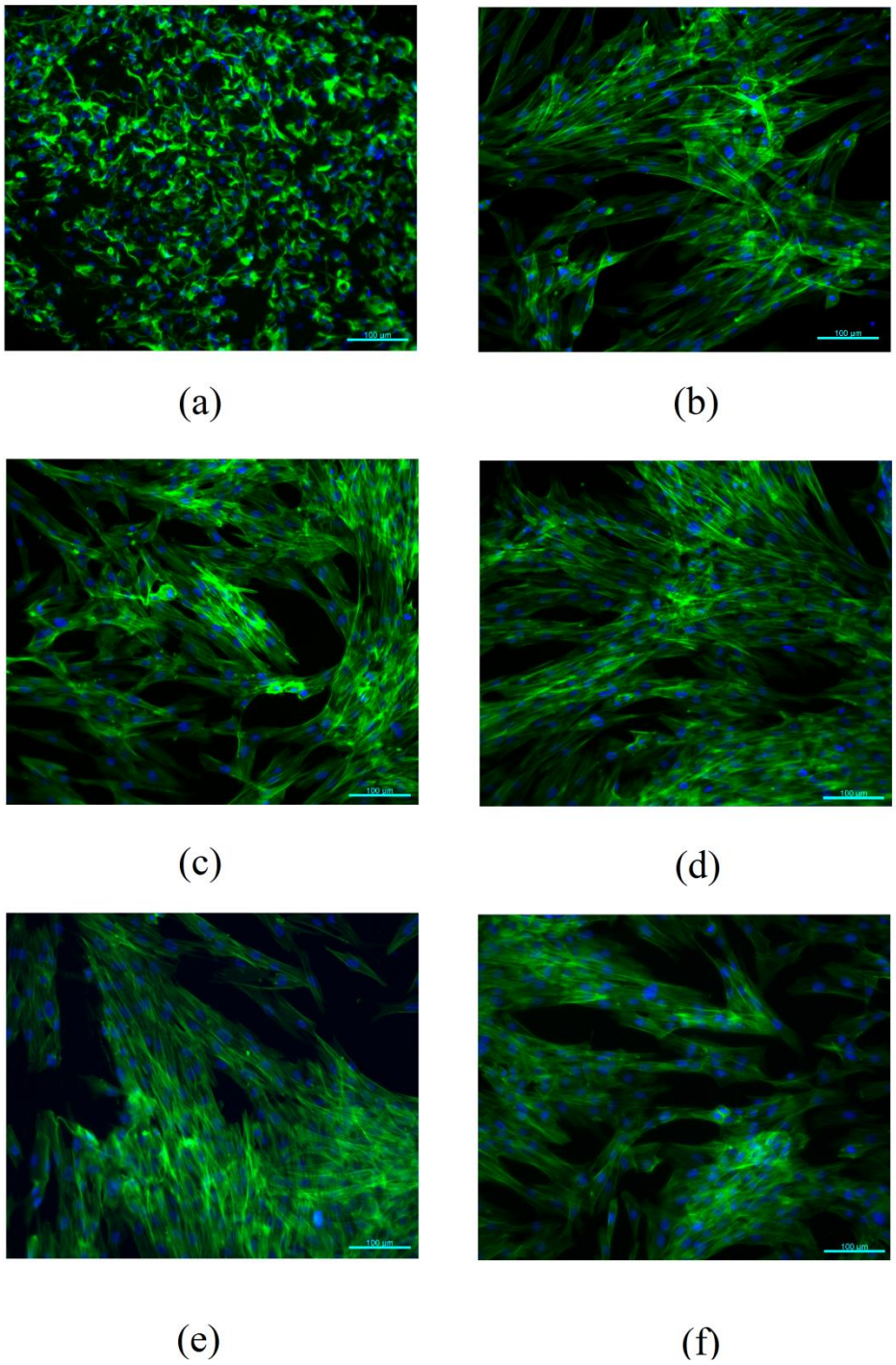

Figure 4.11. Fluorescence images of a) DCP, b) 0.5% SA/DCP, c) 1.0% SA/DCP, d) 2.0% SA/DCP, e) 3.0% SA/DCP cement composites and f) control. Cytoskeleton was stained with Alexa Flour 488-phalloidin (green) and cell nuclei were stained with DAPI (blue). Scale bars are 100µm. Magnification 20x.

CHAPTER 5

CONCLUSION AND RECOMMENDATIONS FOR FUTURE WORKS

5.1. FINDINGS OF THE THESIS

The main purpose of this thesis was to investigate the effect of SA addition on microstructural, mechanical, and biological properties of DCP. A pure phase of DCP (Monetite) and SA doped DCP cement composites were prepared. Incorporating different fractions of SA into DCP resulted in (i) diminished lattice parameters of DCP crystals, (ii) inhibited growth of DCP particles along with no effect on the shape of particles, (iii) rose setting time and improved degree of injectability, (iv) improved degradation rate of DCP scaffolds, (v) improved compressive strength and (vi) increased cell (DPSCs) availability ratio and no influence was observed on cells shape, confirming the *in vitro* biocompatibility of the materials. Finally, DCP composite cements containing 0.5% of SA are found as promising fillers of bone defect and voids.

5.2. SUGGESTED FUTURE WORK

The DCP and SA/DCP cement composites prepared in this thesis have shown good *in vitro* bioactivity, *in vitro* mechanical analysis and *in vitro* biocompatibility is therefore considered a potential candidate in various orthopedics and dental applications. However, their ultimate use as a bone graft material is subjected to successfully establishing biocompatibility, *in vivo* bioactivity and toxicity of these materials.

REFERENCES

Abdel-Fattah, W. I., Reicha, F. M., & Elkhooly, T. A. (2008). Nano-beta-tricalcium phosphates synthesis and biodegradation: 1. Effect of microwave and SO_4^{2-} ions on β-TCP synthesis and its characterization. ***Biomedical Materials***, *3*(3).

Ambard, A. J., & Mueninghoff, L. (2006). Calcium phosphate cement: Review of mechanical and biological properties. ***Journal of Prosthodontics***, *15*(5), 321–328.

Arora, M., Chan, E. K. S., Gupta, S., & Diwan, A. D. (2013). Polymethylmethacrylate bone cements and additives: A review of the literature. ***World Journal of Orthopaedics***, *4*(2), 67–74.

Aurobind, S. V., Amirthalingam, K. P., & Gomathi, H. (2006). Sol-gel based surface modification of electrodes for electro analysis. ***Advances in Colloid and Interface Science***, *121*(1–3), 1–7.

Aydogdu, H., Keskin, D., Baran, E.T., Tezcaner, A. (2016). Pullulan microcarriers for bone tissue regeneration, ***Materials Science and Engineering****: C*, 63 439-449.

Bohner, M. (2010). Design of ceramic-based cements and putties for bone graft substitution. ***European Cells and Materials***, *20*, 1–12.

Bt Ibrahim, S. F., Mohd Azam, N. A. N., & Mat Amin, K. A. (2019). Sodium alginate film: The effect of crosslinker on physical and mechanical properties. ***IOP Conference Series: Materials Science and Engineering***, 509:012063.

Castilho, M., Rodrigues, J., Pires, I., Gouveia, B., Pereira, M., Moseke, C., … Vorndran, E. (2015). Fabrication of individual alginate-TCP scaffolds for bone tissue engineering by means of powder printing. ***Biofabrication***, *7*(1), 15004.

Chang, M. C. (2016). Use of wet chemical method to prepare β tri-calcium phosphates having macro- and nano-crystallites for artificial bone. ***Journal of the Korean Ceramic Society***, *53*(6), 670–675.

Chen, B., Zhang, Z., Zhang, J., Lin, Q., & Jiang, D. (2008). Fabrication and mechanical properties of β-TCP pieces by gel-casting method. ***Materials Science and Engineering C***, *28*(7), 1052–1056.

Chen, C. Y., Ke, C. J., Yen, K. C., Hsieh, H. C., Sun, J. S., & Lin, F. H. (2015). 3D porous calcium-alginate scaffolds cell culture system improved human osteoblast cell clusters for cell therapy. ***Theranostics***, *5*(6), 643–655.

Chow, L. C., & Brown, W. E. (1986). A new calcium phosphate, water-setting cement. In P. W. Brown (Ed.), ***Cements Research Progress*** (pp. 352–379). Westerville: American Ceramic Society.

Dabiri, S. M. H., Lagazzo, A., Barberis, F., Farokhi, M., Finocchio, E., & Pastorino, L. (2016). Characterization of alginate-brushite in-situ hydrogel composites. ***Materials Science and Engineering C***, *67*, 502–510.

Dabiri, S.H., Lagazzo, A., Aliakbarian, B., Mehrjoo, M., Finocchio, E., Pastorino, L. (2019). Fabrication of alginate modified brushite cement impregnated with antibiotic: Mechanical, thermal, and biological characterizations, ***Journal of Biomedical Materials Research Part A***, 107 2063-2075.

Dai, H., Huang, A., Wu, Y., & Li, S. (2016). Synthesis and characterization of mesoporous β-tricalcium phosphate powder by microemulsion technique. In ***Front. Bioeng. Biotechnol. Conference***, *10th World Biomaterials Congress*.

De Campos, M., Müller, F. A., Bressiani, A. H. A., Bressiani, J. C., & Greil, P. (2007). Sonochemical synthesis of calcium phosphate powders. ***Journal of Materials Science: Materials in Medicine***, *18*(5), 669–675.

Desai, T. R., Bhaduri, S. B., & Tas, A. C. (2007). A self-setting, monetite (CaHPO4) cement for skeletal repair. ***Advances in Bioceramics and Biocomposites II***, *3*, 61–69.

Djošić, M. S., Mišković-Stanković, V. B., Milonjić, S., Kačarević-Popović, Z. M., Bibić, N., & Stojanović, J. (2008). Electrochemical synthesis and characterization of hydroxyapatite powders. ***Materials Chemistry and Physics***, *111*(1), 137–142.

Dorozhkin, S. V., & Epple, M. (2002). Biological and medical significance of calcium phosphates. ***Angewandte Chemie - International Edition***, *41*(17), 3130–3146.

Dumitraş, D. G., Marincea, Ş., & Fransolet, A. M. (2004). Brushite in the bat guano deposit from the "dry" Cioclovina Cave (Sureanu Mountains, Romania). ***Neues Jahrbuch Für Mineralogie - Abhandlungen***, *180*(1), 45–64.

El Briak, H., Durand, D., & Boudeville, P. (2008). Study of a hydraulic DCPA/CaO-based cement for dental applications. ***Journal of Materials Science: Materials in Medicine***, *19*(2), 737–744.

Farahani, H. J., Peterson, G. A., & Westfall, D. G. (2012). ***Calcium orthophosphates: applications in nature, biology, and medicine***. (Vol. 64).

Fathi, M., Yacoubi, A. El, Massit, A., Chafik, B., & Idrissi, E. (2015). Wet chemical method for preparing high purity β and α-tricalcium phosphate crystalline powders. ***International Journal of Scientific & Engineering Research***, *6*(6), 139–143.

Fomin, A. S., Fadeeva, I. V., Filippov, Y. Y., Kovalkov, V. K., Grigoryeva, M. A., Shvorneva, L. I., & Barinov, S. M. (2017). Brushite cement based on β-TCP for orthopedics. ***Inorganic Materials: Applied Research***, *8*(2), 292–295.

Gan, Y. X., Jayatissa, A. H., Yu, Z., Chen, X., & Li, M. (2020). Hydrothermal Synthesis of Nanomaterials. ***Journal of Nanomaterials Special***, 1-3.

Gholizadeh, B. S., Buazar, F., Hosseini, S. M., & Mousavi, S. M. (2018). Enhanced antibacterial activity, mechanical and physical properties of alginate/hydroxyapatite bionanocomposite film. ***International Journal of Biological Macromolecules***, *116*(2017), 786–792.

Ginebra, M., & Montufar, E. B. (2019). Cements as bone repair materials. In ***Bone Repair Biomaterials*** (pp. 233–271).

Ginebra, M. P. (2008). Calcium phosphate bone cements. ***Orthopaedic Bone Cements***, 206–230.

Gómez, E., Martín, M., Arias, J., & Carceller, F. (2005). Clinical applications of Norian SRS (calcium phosphate cement) in craniofacial reconstruction in children: Our experience at Hospital la Paz since 2001. ***Journal of Oral and Maxillofacial Surgery***, *63*(1), 8–14.

Grigoraviciute-Puroniene, I., Tsuru, K., Garskaite, E., Stankeviciute, Z., Beganskiene, A., Ishikawa, K., & Kareiva, A. (2017). A novel wet polymeric precipitation synthesis method for monophasic β-TCP. ***Advanced Powder Technology***, *28*(9), 2325–2331.

Hattersley, G., Kerby, J. A., & Chambers, T. J. (1991). Identification of osteoclast precursors in multilineage hemopoietic colonies. ***Endocrinology***, *128*(1), 259–262.

Huan, Z., & Chang, J. (2009). Novel bioactive composite bone cements based on the β-tricalcium phosphate-monocalcium phosphate monohydrate composite cement system. ***Acta Biomaterialia***, *5*(4), 1253–1264.

Ishikawa, K., Miyamoto, Y., Takechi, M., Toh, T., Kon, M., Nagayama, M., & Asaoka, K. (1997). Non-decay type fast-setting calcium phosphate cement: Hydroxyapatite putty containing an increased amount of sodium alginate. ***Journal of Biomedical Materials Research***, *36*(3), 393–399.

Ji, C., & Ahn, J. G. (2010). Clinical experience of the brushite calcium phosphate cement for the repair and augmentation of surgically induced cranial defects following the pterional craniotomy. ***Journal of Korean Neurosurgical Society***, *47*(3), 180–184.

Jin, H.-H., Kim, D.-H., Kim, T.-W., Shin, K.-K., Jung, J.S., Park, H.-C., Yoon, S.-Y. (2012). In vivo evaluation of porous hydroxyapatite/chitosan–alginate composite scaffolds for bone tissue engineering, ***International journal of biological macromolecules***, 51 1079-1085.

Jinawath, S., Pongkao, D., Suchanek, W., & Yoshimura, M. (2001). Hydrothermal synthesis of monetite and hydroxyapatite from monocalcium phosphate monohydrate. ***International Journal of Inorganic Materials***, *3*(7), 997–1001.

Judet, J., & Judet, R. (1950). The use of an artificial femoral head for arthroplasty of the hip joint. ***The Journal of Bone and Joint Surgery***, *32 B*(2), 166–173.

Julien, M., Khairoun, I., LeGeros, R. Z., Delplace, S., Pilet, P., Weiss, P., … Guicheux, J. (2007). Physico-chemical-mechanical and *in vitro* biological properties of calcium phosphate cements with doped amorphous calcium phosphates. ***Biomaterials***, *28*(6), 956–965.

Klammert, U., Reuther, T., Jahn, C., Kraski, B., Kübler, A. C., & Gbureck, U. (2009). Cytocompatibility of brushite and monetite cell culture scaffolds made by three-dimensional powder printing. ***Acta Biomaterialia***, *5*(2), 727–734.

Kohn, M. J., Rakovan, J., & Hughes, J. M. (2002). Phosphates – Geochemical, Geobiological, and Materials Importance. ***Reviews in Mineralogy and Geochemistry***, *48*, 631–672.

Koju, N., Sikder, P., Gaihre, B., & Bhaduri, S. B. (2018). Smart injectable self-setting monetite based bioceramics for orthopedic applications. ***Materials***, *10*(7), 1–18.

Kong, X. D., Sun, X. D., Lu, J. B., & Cui, F. Z. (2005). Mineralization of calcium phosphate in reverse microemulsion. ***Current Applied Physics***, *5*(5), 519–521.

Kossler, W., & Fuchs, J. (2009). Calcium orthophosphates as biomaterials and bioceramics. In ***Bioceramics Properties, Characterizations, and Applications*** (Vol. 97402, pp. 65–159). Nova Science Publishers.

Kouassi, M., Michaïlesco, P., Lacoste-Armynot, A., & Boudeville, P. (2003). Antibacterial effect of a hydraulic calcium phosphate cement for dental applications. ***Journal of Endodontics***, *29*(2), 100–103.

Krauklis, A. E., Kreicbergs, I., & Dreyer, I. (2018). Modified ginstling–brounshtein model for wet precipitation synthesis of hydroxyapatite: Analytical and experimental study. ***Acta of Bioengineering and Biomechanics***, *20*(4), 47–57.

Kreidler, E. R., & Hummel, F. (1967). Phase Relationships in the System SrO-P,O, and the Influence of Water Vapor on the Formation of Sr,P,O,. In ***Inorganic Chemistry*** (Vol. 6, pp. 884–891).

Kuhn, K.-D. (2009). Properties of Bone Cement: What is Bone Cement? ***The Well-Cemented Total Hip Arthroplasty: Theory and Practice***, 52–59.

Laino, G., Graziano, A., D'Aquino, R., Pirozzi, G., Lanza, V., Valiante, S., … Papaccio, G. (2006). An approachable human adult stem cell source for hard-tissue engineering. ***Journal of Cellular Physiology***, *206*(3), 693–701.

Lee, G. S., Park, J. H., Won, J. E., Shin, U. S., & Kim, H. W. (2011). Alginate combined calcium phosphate cements: Mechanical properties and *in vitro* rat bone marrow stromal cell responses. ***Journal of Materials Science: Materials in Medicine***, *22*(5), 1257–1268.

Lee, K. Y., & Mooney, D. J. (2012). Alginate: Properties and biomedical applications. ***Progress in Polymer Science (Oxford)***, *37*(1), 106–126.

Lee, M.N., Hwang, H.-S., Oh, S.-H., Roshanzadeh, A., Kim, J.-W., Song, J.H., Kim, E.-S., Koh, J.-T. (2018). Elevated extracellular calcium ions promote proliferation and migration of mesenchymal stem cells via increasing osteopontin expression, ***Experimental & molecular medicine***, 50 1-16.

Lewis, G. (1997). Properties of acrylic bone cement: State of the art review. ***Journal of Biomedical Materials Research***, *38*(2), 155–182.

Liao, C. J., Lin, F. H., Chen, K. S., & Sun, J. S. (1999). Thermal decomposition and reconstitution of hydroxyapatite in air atmosphere. ***Biomaterials***, *20*(19), 1807–1813.

Luo, J., Engqvist, H., & Persson, C. (2018). A ready-to-use acidic, brushite-forming calcium phosphate cement. ***Acta Biomaterialia***, *81*, 304–314.

Martin, R. B. (2003). Bones: Structure and mechanics. ***Journal of Biomechanics***, *9781400849*, 893–894.

Mathew, M., & Takagi, S. (2001). Structures of biological minerals in dental research. ***Journal of Research of the National Institute of Standards and Technology***, *106*(1), 1035–1044.

McHugh, D. J. (2003). A guide to the seaweed industry. ***FAO Fisheries Technical Paper*** 441, Rome (pp. 39–49).

McMahon, S., Hawdon, G., Bare, J., Sim, Y., Bertollo, N., & Walsh, W. R. (2012). Thermal necrosis and PMMA – a cause for concern? ***Orthopaedic Proceedings***, *94-B*(23), 64.

Mhla, E., & Koutsoukos, P. G. (2017). Heterogeneous crystallization of calcium hydrogen phosphate anhydrous (monetite). ***Colloids and Surfaces A: Physicochemical and Engineering Aspects***, *513*, 125–135.

Mirhadi, B., Mehdikhani, B., & Askari, N. (2011). Synthesis of nano-sized β-tricalcium phosphate via wet precipitation. ***Processing and Application of Ceramics***, *5*(4), 193–198.

Moreno, D., Vargas, F., Ruiz, J., & López, M. E. (2019). Solid-state synthesis of alpha tricalcium phosphate for cements used in biomedical applications. ***Boletín de La Sociedad Española de Cerámica y Vidrio***, 0–7.

Motameni, A., Dalgic, A.D., Alshemary, A.Z., Keskin, D., Evis, Z. (2020). Structural and biological analysis of mesoporous lanthanum doped βTCP for potential use as bone graft material, ***Materials Today Communications***, 101151.

Nandini, Vv., Venkatesh, Kv., & Nair, Kc. (2008). Alginate impressions: A practical perspective. ***Journal of Conservative Dentistry***, *11*(1), 37.

Ni, P., Bi, H., Zhao, G., Han, Y., Wickramaratne, M.N., Dai, H., Wang, X. (2019). Electrospun preparation and biological properties *in vitro* of polyvinyl alcohol/sodium alginate/nano-hydroxyapatite composite fiber membrane, ***Colloids and Surfaces B: Biointerfaces***, 173, 171-177.

Pandi, K., & Viswanathan, N. (2014). Synthesis of alginate bioencapsulated nano-hydroxyapatite composite for selective fluoride sorption. ***Carbohydrate Polymers***, *112*, 662–667.

Perez, R. A., Kim, H. W., & Ginebra, M. P. (2012). Polymeric additives to enhance the functional properties of calcium phosphate cements. ***Journal of Tissue Engineering***, *3*(1), 1–20.

Pikis, S., Goldstein, J., & Spektor, S. (2015). Potential neurotoxic effects of polymethylmethacrylate during cranioplasty. ***Journal of Clinical Neuroscience***, *22*(1), 139–143.

Qadir, M. A., Ahmed, M., Ahmed, S., & Iftikhar-Ul-Haq. (2014). Synthesis of dicalcium phosphate used as feed additive for animals from phosphate rock as potential cost-effective raw material. ***International Journal of Chemical Sciences***, *12*(1), 111–120.

Rad, R. M., Alshemary, A.Z., Evis, Z., Keskin, D., Altunbaş, K., Tezcaner, A. (2018). Structural and biological assessment of boron doped bioactive glass nanoparticles for dental tissue applications, ***Ceramics International***, 44 9854-9864.

Rahaman, M. N. (2014). ***Bioactive ceramics and glasses for tissue engineering***. ***Tissue Engineering Using Ceramics and Polymers*** (2nd ed., pp. 67–114). Elsevier Inc.

Ramesh, S., Adzila, S., Jeffrey, C. K. L., Tan, C. Y., Purbolaksono, J., Noor, A. M., … Teng, W. D. (2013). Properties of hydroxyapatite synthesize by wet chemical method. ***Journal of Ceramic Processing Research***, *14*(4), 448–452.

Rani, P., Pal, P., Panday, J. P., Mishra, S., & Sen, G. (2019). Alginic Acid Derivatives: Synthesis, Characterization and Application in Wastewater Treatment. ***Journal of Polymers and the Environment***, *27*(12), 2769–2783.

Raynaud S., Champion, E., Bernache-Assollant, D., & Thomas, P. (2002). Calcium phosphate apatites with variable Ca/P atomic ratio I. Synthesis, characterisation and thermal stability of powders. ***Biomaterials***, *23*(1), 1065–1072.

Ricker, A., Liu-Snyder, P., & Webster, T. J. (2008). The influence of nano MgO and $BaSO_4$ particle size additives on properties of PMMA bone cement. ***International Journal of Nanomedicine***, *3*(1), 125–132.

Rodríguez-Lugo, V., Karthik, T. V. K., Mendoza-Anaya, D., Rubio-Rosas, E., Villaseñor Cerón, L. S., Reyes-Valderrama, M. I., & Salinas-Rodríguez, E. (2018). Wet chemical synthesis of nanocrystalline hydroxyapatite flakes: Effect of pH and sintering temperature on structural and morphological properties. ***Royal Society Open Science***, *5*(8).

Rohanizadeh, R., & LeGeros, R. Z. (2008). Novel method of hydroxyapatite coating on titanium using chemical deposition. ***Key Engineering Materials***, *361-363 I*, 617–620.

Saleh, A.T., Ling, L.S., Hussain, R. (2016) Injectable magnesium-doped brushite cement for controlled drug release application, ***Journal of materials science***, 51 7427-7439.

Saleh, T. A., Majeed, S., Nayak, A., & Bhushan, B. (2017). Principles and advantages of microwave- assisted methods for the synthesis of nanomaterials for water purification. ***Advanced Nanomaterials for Water Engineering, Treatment, and Hydraulics***, 40–57.

Sanosh, K. P., Chu, M., Balakrishnan, A., Kim, T. N., & Cho, S. (2010). Sol – gel synthesis of pure nano sized b -tricalcium phosphate crystalline powders. ***Current Applied Physics***, *10*(1), 68–71.

Severino, P., da Silva, C. F., Andrade, L. N., de Lima Oliveira, D., Campos, J., & Souto, E. B. (2019). Alginate Nanoparticles for Drug Delivery and Targeting. ***Current Pharmaceutical Design***, *25*(11), 1312–1334.

Shahriari, D., Koffler, J., Lynam, D. A., Tuszynski, M. H., & Sakamoto, J. S. (2016). Characterizing the degradation of alginate hydrogel for use in multilumen scaffolds for spinal cord repair. ***Journal of Biomedical Materials Research - Part A***, *104*(3), 611–619.

Shilpa, A., Agrawal, S. S., & Ray, A. R. (2003). Controlled delivery of drugs from alginate matrix. ***Journal of Macromolecular Science - Polymer Reviews***, *43*(2), 187–221.

Shu, Y., Zhou, Y., Ma, P., Li, C., Ge, C., Wang, Y., … Li, J. (2019). Degradation *in vitro* and in vivo of β-TCP/MCPM-based premixed calcium phosphate cement. ***Journal of the Mechanical Behavior of Biomedical Materials***, *90*, 86–95.

Shull, K. R. (2012). Materials science: A hard concept in soft matter. ***Nature***, *489*(7414), 36–37.

Sivakumar, G. R., Girija, E. K., Narayana Kalkura, S., & Subramanian, C. (1998). Crystallization and Characterization of Calcium Phosphates: Brushite and Monetite. ***Crystal Research and Technology***, *33*(2), 197–205.

Sridhar, T. M. (2010). Nanobioceramic coatings for biomedical applications. ***Materials Technology***, *25*(3–4), 184–195.

Standard Specification for Acrylic Bone Cement. (2016). ASTM F451-16. West Conshohocken, PA.

Standard Test Method for Time of Setting of Hydraulic-Cement Paste by Gillmore Needles. (2004). ASTM C266-04. ASTM International West Conshohocken.

Suryawanshi, V. B., & Chaudhari, R. T. (2014). Growth and Characterization of Agar Gel Grown Brushite Crystals. ***Indian Journal of Materials Science***, *2014*, 1–6.

Tadashi, K., & Takadama, H. (2006). How useful is SBF in predicting in vivo bone bioactivity. ***Biomaterials***, *27*, 2907–2915.

Taha, A., Akram, M., Jawad, Z., Alshemary, A. Z., & Hussain, R. (2017). Strontium doped injectable bone cement for potential drug delivery applications. ***Materials Science and Engineering C***, *80*, 93–101.

Tamimi, F., Torres, J., Bettini, R., Ruggera, F., Rueda, C., López-Ponce, M., & Lopez-Cabarcos, E. (2008). Doxycycline sustained release from brushite cements for the treatment of periodontal diseases. ***Journal of Biomedical Materials Research - Part A***, *85*(3), 707–714.

Tamimi, F., Torres, J., Gbureck, U., Lopez-Cabarcos, E., Bassett, D. C., Alkhraisat, M. H., & Barralet, J. E. (2009a). Craniofacial vertical bone augmentation: A comparison between 3D printed monolithic monetite blocks and autologous onlay grafts in the rabbit. ***Biomaterials***, *30*(31), 6318–6326.

Tamimi, F., Torres, J., Lopez-Cabarcos, E., Bassett, D. C., Habibovic, P., Luceron, E., & Barralet, J. E. (2009b). Minimally invasive maxillofacial vertical bone augmentation using brushite based cements. ***Biomaterials***, *30*(2), 208–216.

Tas, A. C. (2009). Monetite ($CaHPO_4$) synthesis in ethanol at room temperature. ***Journal of the American Ceramic Society***, *92*(12), 2907–2912.

Torres, M. L., Fernandez, J. M., Dellatorre, F. G., Cortizo, A. M., & Oberti, T. G. (2019). Purification of alginate improves its biocompatibility and eliminates cytotoxicity in matrix for bone tissue engineering. ***Algal Research***, *40*, 101499.

Turco, G., Marsich, E., Bellomo, F., Semeraro, S., Donati, I., Brun, F., Grandolfo, M., Accardo, A., & Paoletti, S. (2009). Alginate/hydroxyapatite biocomposite for bone ingrowth: a trabecular structure with high and isotropic connectivity, ***Biomacromolecules***, 10 1575-1583.

Unosson, J. E., Persson, C., & Engqvist, H. (2015). An evaluation of methods to determine the porosity of calcium phosphate cements. ***Journal of Biomedical Materials Research - Part B Applied Biomaterials***, *103*(1), 62–71.

Vaishya, R., Chauhan, M., & Vaish, A. (2013). Bone cement. ***Journal of Clinical Orthopaedics and Trauma***, *4*(4), 157–163.

Venkatesan, J., Nithya, R., Sudha, P. N., & Kim, S. K. (2014). Role of alginate in bone tissue engineering. In ***Advances in Food and Nutrition Research*** (1st ed., Vol. 73, pp. 45–57). Elsevier Inc.

Wang, L., Shelton, R. M., Cooper, P. R., Lawson, M., Triffitt, J. T., & Barralet, J. E. (2003). Evaluation of sodium alginate for bone marrow cell tissue engineering. ***Biomaterials***, *24*(20), 3475–3481.

Wang, P., Song, Y., Weir, M. D., Sun, J., Zhao, L., Simon, C. G., & Xu, H. H. K. (2016a). A self-setting iPSMSC-alginate-calcium phosphate paste for bone tissue engineering. ***Dental Materials***, *32*(2), 252–263.

Wang, X., Xu, S., Zhou, S., Xu, W., Leary, M., Choong, P., … Xie, Y. M. (2016b). Topological design and additive manufacturing of porous metals for bone scaffolds and orthopaedic implants: A review. ***Biomaterials***, *83*, 127–141.

Yashima, M., & Sakai, A. (2003). High-temperature neutron powder diffraction study of the structural phase transition between α and α′ phases in tricalcium phosphate $Ca_3(PO_4)_2$. ***Chemical Physics Letters***, *372*(5–6), 779–783.

Yashima, M., Sakai, A., Kamiyama, T., & Hoshikawa, A. (2003). Crystal structure analysis of β-tricalcium phosphate $Ca_3(PO_4)_2$ by neutron powder diffraction. *Journal of Solid State Chemistry*, *175*(2), 272–277.

Yu, F., Cui, T., Yang, C., Dai, X., & Ma, J. (2019). κ-Carrageenan/Sodium alginate double-network hydrogel with enhanced mechanical properties, anti-swelling, and adsorption capacity, ***Chemosphere***, 237 124417.

Zhang, F., Chang, J., Lu, J., Lin, K., & Ning, C. (2007). Bioinspired structure of bioceramics for bone regeneration in load-bearing sites. ***Acta Biomaterialia***, *3*(6), 896–904.

Zhang, S., Cui, F., Liao, S., Zhu, Y., & Han, L. (2003). Synthesis and biocompatibility of porous nano-hydroxyapatite/collagen/alginate composite, ***Journal of Materials Science: Materials in Medicine***, 14 641-645.

Zhang, X., & Vecchio, K. S. (2007). Hydrothermal synthesis of hydroxyapatite rods. ***Journal of Crystal Growth***, *308*(1), 133–140.

Zhou, Z., Ye, D., Liang, W.,. Wang, B. & Zhu, Z. (2015). Preparation and characterization of a novel injectable strontium-containing calcium phosphate cement with collagen, ***Chinese Journal of Traumatology***, 18 33-38.

APPENDIX A

CALIBRATION CURVE

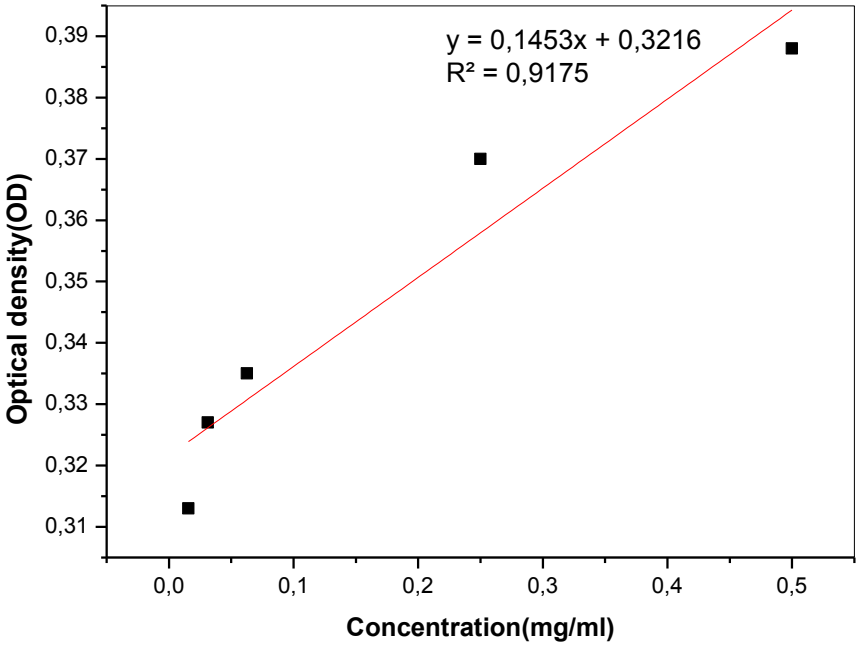

Appendix A.1. Calibration curve of Ca^{2+} ions (mg/mL).

RESUME

Saliha BİLGİN was born in Karabük in 1995 and she graduated first and elementary education in Safranbolu/KARABÜK. She completed high school education in Safranbolu Anatolian High School in 2012. She graduated from Erciyes University, Engineering Faculty, Department of Biomedical Engineering in Kayseri in 2016. She started the master program in Karabük University, Department of Biomedical Engineering in 2016.

CONTACT INFORMATION

Address: Eryaman mah. 324.sok. Kağan apt. 2/2 Etimesgut/ANKARA

E-mail: armagansaliha@gmail.com